



HAL
open science

Spherical oscillations of encapsulated microbubbles: Effect of shell compressibility and anisotropy

Georges Chabouh, Benjamin Dollet, Catherine Quilliet, Gwennou Coupier

► To cite this version:

Georges Chabouh, Benjamin Dollet, Catherine Quilliet, Gwennou Coupier. Spherical oscillations of encapsulated microbubbles: Effect of shell compressibility and anisotropy. *Journal of the Acoustical Society of America*, 2021, 149 (2), pp.1240-1257. 10.1121/10.0003500 . hal-03151985

HAL Id: hal-03151985

<https://hal.science/hal-03151985>

Submitted on 5 Oct 2021

HAL is a multi-disciplinary open access archive for the deposit and dissemination of scientific research documents, whether they are published or not. The documents may come from teaching and research institutions in France or abroad, or from public or private research centers.

L'archive ouverte pluridisciplinaire **HAL**, est destinée au dépôt et à la diffusion de documents scientifiques de niveau recherche, publiés ou non, émanant des établissements d'enseignement et de recherche français ou étrangers, des laboratoires publics ou privés.

Spherical oscillations of encapsulated microbubbles: effect of shell compressibility and anisotropy

Georges Chabouh,¹ Benjamin Dollet,¹ Catherine Quilliet,¹ and Gwennou Coupier^{1, a)}

*Université Grenoble Alpes, CNRS, LIPhy, F-38000 Grenoble,
France*

(Dated: 12 January 2021)

1 We introduce a model that describes spherical oscillations of encapsulated microbub-
2 bles in an unbounded surrounding fluid. A Rayleigh-Plesset-like equation is derived
3 by coupling the Navier-Stokes equation that describes fluid dynamics with the Navier
4 equation that describes solid dynamics via the internal/external boundary conditions.
5 While previous models were restricted to incompressible isotropic shells, the solid shell
6 is modeled here as a compressible viscoelastic isotropic material, then generalised to
7 an anisotropic material. The exact value of the resonance frequency is calculated
8 analytically and the damping constant is computed in the approximation of weak
9 damping. A correction of the widely used Church model for incompressible shells is
10 evidenced, and the effects of shell compressibility and anisotropy are discussed.

^{a)} gwennou.coupier@univ-grenoble-alpes.fr

11 I. INTRODUCTION

12 Various modalities have been used for diagnostic imaging, such as clinical radiography,
13 computed tomography (CT), magnetic resonance imaging (MRI) and ultrasounds (US). Be-
14 ing safe, noninvasive and relatively cheap, US imaging techniques have been much improved
15 by the introduction of ultrasound micron size contrast agents (UCAs). The need of image
16 enhancers was essential because first, human blood within an organ has poor scattering prop-
17 erties and low signal amplitude relative to human tissues, that generate strong echoes, and
18 second, the old-school Doppler technique ([Campbell *et al.*, 1983](#)) could not satisfy anymore
19 the demands, especially in some more complex and confined geometries.

20 The presence of air bubbles inside an injected hand-agitated saline solution during an
21 echocardiography was the first ultrasonic image enhancement technique that was proposed
22 ([Gramiak and Shah, 1968](#)). These bubbles are known as the first generation of UCAs.
23 As they dissolve rapidly in the liquid, a second generation of UCAs was developed, that
24 are made of air bubbles encapsulated by a thin shell: galactose as in Echovist[®] (1991)
25 or albumin (a human protein) as in Albunex[®](1995) or galactose and palmitic acid as in
26 Levovist[®](1995). Finally, the third generation of UCAs includes microbubbles with higher
27 life-time, air being simply replaced by a gas with higher molecular weight, responsible of
28 decreased solubility: SF₆ as in Sonovue[®] (2001), C₃F₈ as in Definity[®](2001) or C₄F₁₀ as in
29 Sonazoid[®](2007). All of these gases are encapsulated by phospholipids. The resulting shells
30 are known as soft-shell UCAs, while the ones made with polymers are known as hard-shell
31 UCAs.

32 UCAs react to high amplitude pulses (1 MPa) of short duration (of the order of the
33 μs). Even in presence of such agents, axial and lateral resolutions of ultrasonic devices used
34 in clinical applications are limited by diffraction, such that the resolution is fixed by the
35 typical wavelength, which lies between 100 μm and 1 mm in practice. This limit has been
36 strikingly overcome recently: by analysing the transient signal re-emitted by UCAs, in-vivo
37 resolution has been decreased to about 10 μm , at a detection frequency high enough to
38 also allow velocity measurement in blood flow by image correlation (Errico *et al.*, 2015).
39 Such a super-resolved technique can also be implemented through a photoacoustic device,
40 where the UCAs are excited by light rather than by sound (Vilov *et al.*, 2017). The scattered
41 ultrasound signal of UCAs has also been recently used to discriminate between two networks
42 topologies, with application to cancerous tumor detection (Mohanty *et al.*, 2019).

43 These recent advances are based on a complex interplay between hardware development
44 and post-processing to extract the relevant information from the acquired signal. The re-
45 sponse of a shelled bubble is strongly dependent on its size and on the shell material proper-
46 ties. While commercial UCAs are quite polydisperse in size, narrowing the size distribution
47 of UCAs appears then as a way to match better the relatively narrow frequency bandwidth
48 of ultrasonic devices with that of the UCAs, thus leading to better sensitivity of the whole
49 detection process. Recent works go in that direction, that make use of shell material of vari-
50 ous types, such as polymers (Liu *et al.*, 2014; Song *et al.*, 2018), phospholipids (Gong *et al.*,
51 2014; Helfield *et al.*, 2014; Lum *et al.*, 2016; Parrales *et al.*, 2014; Segers *et al.*, 2016; 2020;
52 van Rooij *et al.*, 2015) — sometimes forming more than 2 layers (Shafi *et al.*, 2019), silica
53 (Hu *et al.*, 2011) or proteins (Wang *et al.*, 2020). This calls for models of bubble oscillations

54 that are able to describe a wide variety of shell materials. While previous ones are focused on
55 incompressible and isotropic material, we present here a model that includes compressibility
56 and the possibility for spherical UCAs to present different material properties in the radial
57 and orthoradial directions (“transverse isotropic” material), a feature that would naturally
58 occur for layered shells like lipidic ones.

59 Such anisotropy has been shown to greatly influence the buckling process of shells
60 (Munglani *et al.*, 2019; Pitois *et al.*, 2015; Quemeneur *et al.*, 2012).

61 II. PREVIOUS MODELS

62 Since the early work of Besant (1859) who was concerned by the time needed to fill
63 up the empty space of a collapsed bubble and the pressure generated at any point in an
64 incompressible liquid, forced vibrations of bubbles have attracted attention for decades.
65 Giving a simpler derivation of Besant’s results, Lord Rayleigh (1917) generalized the case
66 to a cavity with nonzero pressure, *i.e.* to a gas-filled bubble. The surface tension and the
67 viscosity of the surrounding fluid were taken into account (see Plesset and Prosperetti (1977)
68 for a review), leading to the famous Rayleigh-Plesset equation.

69 In order to take into account the shell encapsulating the microbubble, a semi-empirical
70 model was developed (De Jong *et al.*, 1994; de Jong *et al.*, 1992) by way of the introduction
71 of two *ad-hoc* quantities S_p and S_f that account for the effective elastic and dissipative prop-
72 erties of the interface. Assuming a zero-thickness shell, which is motivated by the proximity
73 between the shell thickness and the molecular scale, other models have introduced rheolog-
74 ical constants that are explicitly related to the expected properties of the shell material.

75 The first approach by Chatterjee and Sarkar (2003) was followed by the models of Sarkar
76 *et al.* (2005) and Marmottant *et al.* (2005). In the latter, a non-linear model is proposed,
77 presenting the elasticity of the shell as an effective surface tension. Its linearized form is
78 equivalent to the de Jong model.

79 In Church (1995), a finite thickness shell was considered. It was assumed to be made of a
80 homogeneous, incompressible and isotropic material, that was described by a Kelvin-Voigt
81 model. This model was linearized relatively to the thickness to radius ratio in Hoff *et al.*
82 (2000), giving rise to the Church-Hoff model. In Morgan *et al.* (2000), thin-shell UCAs were
83 described by a constant thickness model using bulk elasticity and viscosity.

84 Following Marmottant *et al.* (2005), other nonlinear models have been proposed, with a
85 more complex rheological behavior like strain softening and strain hardening (Paul *et al.*,
86 2010; Tsigliferis and Pelekasis, 2008), or shear thinning (Doinikov *et al.*, 2009; Li *et al.*, 2013).

87 III. CONFRONTATION WITH EXPERIMENTS

88 Vibration experiments on UCAs should a priori allow to determine the rheological con-
89 stants of the material, through the chosen model among those cited above, as long as they
90 are not too many. The final goal is usually to choose the best fitting couple of one elastic
91 and one viscous parameter to describe the observed damped signal. This couple is unique
92 for the model selected, for instance, (S_p, S_f) in de Jong *et al.* (1992) model, (G_S, μ_S) in
93 (Church, 1995) model and so on. Note that using finite thickness shell models requires to
94 make assumptions, or additional measurements, to determine the value of the shell thick-

95 ness. In all models, additional assumptions are generally made in order not to consider the
96 inner gas pressure as an unknown to be determined.

97 Several techniques can be used to determine the shell oscillations. In [Gorce *et al.* \(2000\)](#),
98 a batch of encapsulated microbubbles are insonated at frequencies up to 30 MHz, and
99 the viscoelastic parameters are deduced by measuring the attenuation expression. The
100 spectroscopy approach relies on using a high speed camera to directly measure the radial
101 displacement of the UCAs, which is fitted with the theoretical one ([van der Meer *et al.*,
102 2007](#)). Light scattering methods were also developed ([Li *et al.*, 2013](#); [Tu *et al.*, 2009](#)), where
103 the scattering cross section is related to the resonance frequency containing the viscoelastic
104 properties using the Mie scattering theory. A photoacoustic measurement technique was
105 developed in [Lum *et al.* \(2016\)](#). Readers can refer to [Helfield \(2019\)](#); [versluis *et al.* \(2015\)](#)
106 for recent reviews on linear models theory and experimental measuring methods.

107 All the existing linear models are virtually the same, with 2D moduli that can be expressed
108 explicitly in terms of 3D moduli and thickness. Tables [I-IV](#) summarize some experimental
109 estimations of shell properties using the De Jong, Marmottant, Church-Hoff and Sarkar
110 models respectively for different UCAs and using various techniques.

111 Such experiments may also be used to validate the model that is used to describe the
112 results. This requires to determine by another means the rheological properties of the shell
113 material. Such validations are scarce in the literature, and yield only accurate order of mag-
114 nitude so far. The atomic force microscopy (AFM) is a direct approach used to estimate
115 UCAs' properties. However, depending on the model used to extract elastic constants from
116 the force-displacement curve of an AFM, very different values can be found ([Abou-Saleh](#)

117 *et al.*, 2013; Buchner Santos *et al.*, 2012; Lytra *et al.*, 2020; Shafi *et al.*, 2019). This makes
118 the validation of spherical oscillation models a tricky task so far. As an example, in Buch-
119 ner Santos *et al.* (2012) and Lytra *et al.* (2020), values between 8 and 38 MPa are found
120 for the Young modulus E' of a Definity[®] UCA probed by an AFM. For an incompressible
121 material the 2D compression modulus χ_{2D} is $E'd_0$, where d_0 is the shell thickness, estimated
122 to be around 5 nm for such UCAs. This leads to $0.04 < \chi_{2D} < 0.2$ N/m, which is not in
123 agreement with the values around 1 N/m found with the de Jong (Table I) or Marmottant
124 (Table II) model. Note however, that static values of the shell may differ considerably from
125 dynamic values measured in the MHz range.

126 In addition, experimental determinations have lead to unexpected dependencies of the vis-
127 coelastic parameters on shell radius, as also shown in Tables I-III. van der Meer *et al.* (2007)
128 observed a dependence of the shell viscosity on the initial bubble radius using Marmottant
129 model for BR-14[®]. Chetty *et al.* (2008) measured an increase of the shear modulus G'
130 with the radius using Church-Hoff model for Sonovue[®]. Tu *et al.* (2009) and Li *et al.* (2013)
131 measured an increase of the elasticity and the viscosity parameters of the shell with the shell
132 radius, using the linearized Marmottant model for Sonovue[®]. Identical observation where
133 made in Doinikov *et al.* (2009) (lipid encapsulated bubbles with De Jong model), Helfield and
134 Goertz (2013) (Definity[®] with Marmottant model), and Parrales *et al.* (2014) (home-made
135 monodisperse encapsulated microbubbles with the linearized Marmottant model).

136 This dependence on radius of the material properties was not substantiated by physical
137 arguments, suggesting that extra modeling was required.

138 So far, the models have not considered the possible compressibility or anisotropy of the
 139 material constituting the shell. The purpose of the present article is to include these effects
 140 in the model of bubble oscillations and to quantify their influence on the linearized oscillation
 141 properties, i.e. the eigenfrequency and the damping coefficient.

TABLE I. Shell properties estimations using de Jong model (de Jong *et al.*, 1992). f and p are the characteristic frequencies and amplitudes of the acoustic waves used to excite the UCAs. S_p and S_f are the elastic and viscous ad-hoc parameters that are introduced in the model. The intervals for the viscoelastic parameters correspond to cases where dependency on the radius was reported.

UCA	$R_{20}(\mu\text{m})$	$f(\text{MHz})$	$p(\text{kPa})$	S_p (N/m)	S_f (10^{-6}N/m.s)	Method	Reference
SonoVue [®]	0.6 – 4.5	1 – 10	< 10	0.35 – 2.61	0.46 – 3.42	Attenuation	(Gorce <i>et al.</i> , 2000)
Albunex [®]	2.5 – 6	0.7 – 12.5	not known	8	4	Attenuation	(de Jong and Hoff, 1993)
Definity [®]	0.5 – 2.5	12 – 28	25	1.71	0.015	Attenuation	(Goertz <i>et al.</i> , 2007)
	1 – 3	7 – 15	25	1.64	0.15	Attenuation	(Faez <i>et al.</i> , 2011)

142 IV. MODEL

143 We consider an encapsulated gas bubble immersed in an incompressible fluid with a
 144 density ρ_f and a shear viscosity μ_f . The effect of the liquid compressibility could be further
 145 included as described in the work of Prosperetti (1987). The bubble shell is modeled as a
 146 visco-elastic solid of initial thickness d_e . Furthermore, it was shown according to thin shell
 147 theory that a shell made of an homogeneous material with Poisson ratio ν may sustain a

TABLE II. Shell properties estimations using Marmottant model (Marmottant *et al.*, 2005). f and p are the characteristic frequencies and amplitudes of the acoustic waves used to excite the UCAs. Analysis of experiments through the model allow to determine the 2D compression modulus χ_{2D} and the surface dilatational viscosity κ_S . In the linearized version of the model, they are related to the constants introduced by de Jong through $S_p = 2\chi_{2D}$ and $S_f = 12\pi\kappa_S$. The intervals for the viscoelastic parameters correspond to cases where dependency on the radius was reported.

UCA	$R_{20}(\mu\text{m})$	$f(\text{MHz})$	$p(\text{kPa})$	χ_{2D} (N/m)	$\kappa_S(10^{-8}$ N/m.s)	Method	Reference
SonoVue [®]	0.975	2.9	130	1	1.5	Spectroscopy	(Marmottant <i>et al.</i> , 2005)
	0.8 – 3.25	2.5	150	0.024 – 0.87 ^a	0.1 – 3	Light scattering	(Tu <i>et al.</i> , 2009)
	0.75 – 3.25	2.5	150	0.39 – 0.55	0.05 – 2	Light scattering	(Tu <i>et al.</i> , 2011)
	0.8 – 3.25	2.5	150	0.4 – 0.55	0.1 – 3	Light scattering	(Li <i>et al.</i> , 2013)
BR14 [®]	1.9	1.5 – 2.5	< 40	0.54 ^a	2.3	Spectroscopy	(van der Meer <i>et al.</i> , 2007)
Definity [®]	0.72 – 1.4	1	308	0.5 – 0.97	0.01 – 0.9	Light scattering	(Tu <i>et al.</i> , 2011)
	1.4 – 2.8	4 – 13.5	6 – 25	0.5 – 2.5	0.02 – 0.6	Spectroscopy	(Helfield and Goertz, 2007)
Home-made lipid shell	2.9 – 6.3	0.5 – 4	–	0.28 – 0.85	3 – 6	Attenuation	(Parrales <i>et al.</i> , 2014)

^a Linearized version of the model

TABLE III. Shell properties estimations using Church-Hoff model (Hoff *et al.*, 2000). The thickness d_0 is an estimation which is made in each paper. f and p are the characteristic frequencies and amplitudes of the acoustic waves used to excite the UCAs. The intervals for the viscoelastic parameters correspond to cases where dependency on the radius was reported.

UCA	$R_{20}(\mu\text{m})$	$d_0(\text{nm})$	$f(\text{MHz})$	$p(\text{kPa})$	$G'(\text{MPa})$	$\mu_G (\text{Pa.s})$	Method	Reference
SonoVue [®]	1.78	4	2.5	150	20	0.6	Light scattering	(Tu <i>et al.</i> , 2009)
	3 – 5.5	2.5	6.8 – 7.3	40	1.9 – 105	1	Microscopy	(Chetty <i>et al.</i> , 2008)
Sonazoid [®]	1.6	4	2 – 6	300 – 800	52	0.99	Attenuation	(Sarkar <i>et al.</i> , 2005)
Optison [®]	1.5	5 – 10	3.6 – 4.3	100	20.7	1.7	Attenuation	(Chatterjee and Sarkar, 2005)

TABLE IV. Shell properties estimations using Sarkar model (Sarkar *et al.*, 2005). f and p are the characteristic frequencies and amplitudes of the acoustic waves used to excite the UCAs. E^S and κ^S are the surface dilatational elasticity and viscosity respectively introduced in the model.

UCA	$R_{20}(\mu\text{m})$	$f(\text{MHz})$	$p(\text{kPa})$	$E^S (\text{N/m})$	$\kappa^S(10^{-8}\text{N/m.s})$	Method	Reference
Sonazoid [®]	3.2	2 – 6	200 – 600	0.51	1	Attenuation	(Sarkar <i>et al.</i> , 2005)
Home-made	0.7 – 1.5	2.5 – 3	100 – 150	0.02	0.85	Attenuation	(Paul <i>et al.</i> , 2013)
PLA shell							

148 maximum relative loss of volume

$$(\Delta V/V)_b = \sqrt{\frac{3(1-\nu)}{1+\nu}} \frac{d_0}{R_{20}}, \quad (1)$$

149 before it buckles (Hutchinson, 1967; Quilliet, 2012), where d_0 and R_{20} are the shell thickness
150 and external radius at rest, respectively. The first fraction is of order 1, except for exotic val-
151 ues of ν close to -1 . Even for shells happening to be thicker than the commercially available
152 ones, $(\Delta V/V)_b$ is hence reasonably expected not to exceed $1/10$. This point, plus recent
153 experimental results having suggested that pressure-volume relationships obtained within
154 the framework of thin shell theory apply also for thick shells (Coupier *et al.*, 2019), indicates
155 that we may safely consider, here and in the following, that linear elasticity framework is
156 sufficient to describe the spherical behaviour of a wide range of UCAs in the unbuckled
157 regime.

158 A. Quasi-static approximation

159 In the absence of body forces, the equation of motion in the solid (Landau and Lifschitz,
160 1986) reads

$$\rho_S \frac{\partial^2 \mathbf{u}}{\partial t^2} - \nabla \cdot \boldsymbol{\sigma} = 0, \quad (2)$$

161 where ρ_S is the initial density of the solid, \mathbf{u} the displacement field, and $\boldsymbol{\sigma}$ is the Cauchy
162 stress tensor calculated on the actual configuration.

163 If we consider only elastic contributions to the stress, the dimensional analysis of (2)
164 shows that if the parameter $\varepsilon = \omega_0^2 d_e^2 \rho_S / E$, that compares the orders of magnitude of the
165 first and second term in (2), is small, then acceleration can be neglected (see e.g. Langtangen
166 and Pedersen (2016)). Here E is a typical elastic constant of the material, and ω_0 is the
167 (unknown) shell pulsation. Physically, $\sqrt{\varepsilon}$ is the ratio of the typical time scale $\tau_0 = d_e \sqrt{\rho_S / E}$
168 needed for an elastic wave to travel across the shell thickness d_e over the time scale ω_0^{-1} of

169 the motion of the boundary. In general, E is not smaller than 100 MPa for a polymeric
170 material where $d_e \sim 100$ nm, but for lipid shells of thickness of order 5 nm which are made of
171 the type of anisotropic material that we treat later on in this paper, orders of magnitude as
172 low as 100 kPa were proposed for an effective isotropic Young modulus (Shafi *et al.*, 2019).
173 Hence, with $\rho_S \sim 1000$ kg/m³, τ_0 is expected to be smaller than 5×10^{-10} s. This implies
174 that, with ω_0 usually measured or found according to previous models lower than 10 MHz,
175 ε is lower than 10^{-4} .

176 The acceleration term can therefore be neglected for actual UCAs and will be so in the
177 rest of this paper. The resolution of Eq.(2) under this assumption will serve to determine
178 the boundary conditions for the stress in the fluid, in order to determine its acceleration.

179 A problem similar to ours has been widely studied recently, that of a bubble oscillating in
180 a liquid confined by a visco-elastic solid (Doinikov *et al.*, 2018; Doinikov and Marmottant,
181 2018; Vincent and Marmottant, 2017; Wang, 2017). A simplifying hypothesis, that is used
182 in Vincent and Marmottant (2017) and Wang (2017) is to consider that the surrounding
183 solid is not accelerated by the pressure waves. Here, we have shown that this hypothesis
184 holds for our problem, due in particular to the thinness of the shells.

185 Note that the resonance frequency ω_0 is the unknown of this problem, so the validity of
186 the hypothesis has to be checked a posteriori.

187 **B. Stress-strain relation in the solid**

188 We consider the shell as being made of a transverse isotropic material, i.e. whose proper-
189 ties in the orthoradial plane do not depend on the direction considered but can be different

190 from that in the radial direction. The elastic properties of such a material are character-
 191 ized by five independent elastic constants. The stress-strain relationship can be written as
 192 (Lubarda and Chen, 2008):

$$\begin{aligned} \sigma_{ij}^{el} = & \lambda \epsilon_{kk} \delta_{ij} + 2\mu \epsilon_{ij} + 2(\mu_0 - \mu) (\delta_{i_0 i} \epsilon_{i_0 j} + \delta_{i_0 j} \epsilon_{i_0 i}) \\ & + \alpha (\epsilon_{i_0 i_0} \delta_{ij} + \delta_{i_0 i} \delta_{i_0 j} \epsilon_{kk}) + \beta \delta_{i_0 i} \delta_{i_0 j} \epsilon_{i_0 i_0}, \end{aligned} \quad (3)$$

193 where ϵ is the strain tensor, λ is the first Lamé coefficient, μ the shear modulus in the plane
 194 of isotropy, μ_0 the out-of-plane shear modulus, and α and β two other coefficients. The
 195 direction i_0 points the axis of transverse isotropy. For an isotropic material, $\alpha = \beta = 0$
 196 and $\mu_0 = \mu$. For radial displacements, the elastic Cauchy stress tensor has only diagonal
 197 components given by

$$\begin{cases} \sigma_{rr}^{el} = (\lambda + 4\mu_0 - 2\mu + 2\alpha + \beta) \epsilon_{rr} + 2(\lambda + \alpha) \epsilon_{\theta\theta} \\ \sigma_{\theta\theta}^{el} = \sigma_{\phi\phi}^{el} = (\lambda + \alpha) \epsilon_{rr} + 2(\lambda + \mu) \epsilon_{\theta\theta} \end{cases}, \quad (4)$$

198 with $\epsilon_{rr} = \partial u / \partial r$ and $\epsilon_{\theta\theta} = \epsilon_{\phi\phi} = u/r$, where $u = u(r, t)$ is the Eulerian radial displacement
 199 in the shell.

200 The viscoelastic properties of the material are described by the generalized Kelvin-Voigt
 201 model (Thompson and Kelvin, 1865; Voigt, 1892) where the complete strain tensor reads
 202 $\boldsymbol{\sigma} = \boldsymbol{\sigma}^{el} + \boldsymbol{\sigma}^{visc}$, where $\boldsymbol{\sigma}^{visc}$ is the viscous stress. For a transverse anisotropic material,
 203 integrating a thermodynamical consistent model (Dalenbring, 2002) based on the augmented
 204 Hooke's law (AHL) (Dovstam, 1995) in this fluid-structure interaction problem requires
 205 finite elements implementation. Another approach may be to consider viscosity effect for
 206 only some components of the stress tensor (Lubarda and Asaro, 2014).

207 We will therefore consider two cases in this paper, both going one step further compared
 208 to the model by [Church \(1995\)](#) that considers an isotropic and incompressible material:

- 209 1. A visco-elastic isotropic material, that can be compressible,
- 210 2. An anisotropic, purely elastic, material which is transversely isotropic and compress-
 211 ible.

212 In the case of an isotropic linear material, the elastic stress reads

$$\left\{ \begin{array}{l} \sigma_{rr}^{el} = (K' + \frac{4}{3}G') \epsilon_{rr} + 2(K' - \frac{2}{3}G') \epsilon_{\theta\theta} \\ \sigma_{\theta\theta}^{el} = \sigma_{\phi\phi}^{el} = (K' - \frac{2}{3}G') \epsilon_{rr} + 2(K' + \frac{1}{3}G') \epsilon_{\theta\theta} \end{array} \right. , \quad (5)$$

213 where we have introduced the shear modulus $G' = \mu$ and the bulk modulus $K' = \lambda + \frac{2}{3}\mu$.
 214 Both are *a-priori* functions of the oscillation frequency, which would call for the resolution
 215 of a self-consistency equation when the oscillation frequency will be eventually found as a
 216 function of, in particular, these elastic constants. We introduce the Kelvin-Voigt viscous
 217 stress σ^{visc} whose expression is similar to that of the elastic stress:

$$\left\{ \begin{array}{l} \sigma_{rr}^{visc} = (\mu_K + \frac{4}{3}\mu_G) \dot{\epsilon}_{rr} + 2(\mu_K - \frac{2}{3}\mu_G) \dot{\epsilon}_{\theta\theta} \\ \sigma_{\theta\theta}^{visc} = \sigma_{\phi\phi}^{visc} = (\mu_K - \frac{2}{3}\mu_G) \dot{\epsilon}_{rr} + 2(\mu_K + \frac{1}{3}\mu_G) \dot{\epsilon}_{\theta\theta} \end{array} \right. \quad (6)$$

218 The viscosities μ_K and μ_G describe the friction losses due to volume changes and shear,
 219 respectively. Little is known, in general, about the values of the loss moduli and, in par-
 220 ticular, the “viscous Poisson ratio” whose definition may vary depending on the authors
 221 ([Lakes and Wineman, 2006](#)). Its determination generally requires to perform two inde-
 222 pendent experiments aiming at determining, e.g., a shear loss modulus G'' and a traction

223 loss modulus E'' (see, e.g. [Guillot and Trivett \(2011\)](#)). From a modelling perspective,
 224 one approach consists in following [Lemaitre and Chaboche \(1994\)](#) where it is assumed ,
 225 with no explicit justification that the ratio μ_K/μ_G is equal to K'/G' which amounts to say
 226 that the viscous Poisson ratio that would characterize a ratio of strain rates is equal to
 227 the elastic Poisson ratio that characterises the ratio of strains ([Linn *et al.*, 2013](#); [von Ende
 228 *et al.*, 2011](#)). Without this assumption, and considering an AHL model as in [Tschoegl *et al.*
 229 \(2002\)](#), [Pritz \(2009\)](#) have proposed bounds for the potential values of the loss moduli for
 230 materials with a positive Poisson ratio and a low enough shear loss factor. They show that
 231 $2/3 < K''/G'' < 1$ which, for a sinusoidal signal of given pulsation w_0 , amounts to the tight
 232 inequalities $2/3 < \mu_K/\mu_G < 1$. We discuss these two assumptions in the discussion (Sec.
 233 [V J](#)), but one should keep in mind that the difficulties in characterizing accurately two dissi-
 234 pation constants in viscoelastic materials, whose properties are often frequency dependent,
 235 must lead to consider the aforementioned relationships as pure hypotheses as for now.

236 V. ISOTROPIC COMPRESSIBLE SHELL

237 A. Deformation in the solid

238 The Eulerian radial displacement u within the shell is defined on the actual configuration
 239 as the variation from an unstrained position holding no stress within the shell:

$$u(r, t) = r - r_e, \tag{7}$$

240 where r is the actual position of a material particle located at r_e in the reference configura-
 241 tion.

242 The radial displacement $u(r, t)$ is then calculated by solving Eq. (2) in the quasi-static
 243 approximation:

$$[\nabla \cdot (\boldsymbol{\sigma}^{el} + \boldsymbol{\sigma}^{visc})]_r = 0. \quad (8)$$

244 The ratio between the viscous and the elastic terms in the above equation is given by the
 245 ratio between the loss and storage moduli. Previous experimental studies on existing UCAs
 246 show that the ratio between the viscosity and the storage modulus is of order $10^{-8} - 10^{-9}$ s
 247 (see values in tables I–IV) therefore $\omega_0 \tau_S$ is often small, which we will take as a hypothesis
 248 in the following.

249 For an isotropic solid, from $[\nabla \cdot \boldsymbol{\sigma}]_r = \frac{\partial \sigma_{rr}}{\partial r} + \frac{2}{r} (\sigma_{rr} - \sigma_{\theta\theta})$ and using Eqs. (5) and (6), we
 250 are lead to solve:

$$\left(\frac{\partial^2}{\partial r^2} + \frac{2}{r} \frac{\partial}{\partial r} - \frac{2}{r^2} \right) (u + \tau_S \dot{u}) = 0, \quad (9)$$

251 with:

$$\tau_S = \frac{\mu_M}{M'}, \quad M' = K' + \frac{4}{3}G', \quad \mu_M = \mu_K + \frac{4}{3}\mu_G. \quad (10)$$

252 The solutions of Eq. (9) can be written:

$$u(r, t) = a(t)r + \frac{b(t)}{r^2} + A(r)e^{-t/\tau_S}, \quad (11)$$

253 where the term in $A(r)$ characterizes the internal relaxation within the shell. Note that since
 254 $\omega_0 \tau_S$ is small, this term will marginally contribute to the overall response of the shell, and
 255 we shall therefore place ourselves in the conditions where it is zero.

256 The two variables $a(t)$ and $b(t)$ depend on the long time $t \gg \tau_S$ associated with the
 257 variations of the boundary conditions. We first express them as functions of $R_1(t)$ and
 258 $R_2(t)$, respectively the internal and external radii of the shell, which are our variables of

259 interest. This is achieved thanks to Eq.(7), which leads to $u(R_i) = R_i(t) - R_{ie}$, for $i = 1, 2$.
 260 R_{1e} and R_{2e} are the values of the radii in the unstrained case, and R_{10} and R_{20} their values at
 261 equilibrium in the fluid, which may differ from R_{1e} and R_{2e} , notably because of hydrostatic
 262 pressure. We find:

$$a(t) = \frac{R_2^2(t)[R_2(t) - R_{2e}] - R_1^2(t)[R_1(t) - R_{1e}]}{R_2^3(t) - R_1^3(t)}, \quad (12)$$

263 and:

$$b(t) = \frac{R_1^2(t)R_2^2(t)}{R_2^3(t) - R_1^3(t)} \times \{R_2(t)[R_1(t) - R_{1e}] - R_1(t)[R_2(t) - R_{2e}]\}. \quad (13)$$

264 Note that a and b are of order 1 relatively to the displacements at the boundaries, in
 265 agreement with the linear elastic theory used here to characterize the deformation tensor.

266 B. Velocity in the solid

267 The velocity field in the shell \mathbf{v}_s is the material derivative of the Eulerian displacement
 268 $\mathbf{u}(r, t)$:

$$\mathbf{v}_s(r, t) = \frac{D\mathbf{u}}{Dt} = \frac{\partial\mathbf{u}}{\partial t} + \nabla\mathbf{u} \cdot \mathbf{v}_s(r, t). \quad (14)$$

269 For small deformations, $|\nabla\mathbf{u}| \ll 1$, the radial component of the velocity v_s thus can be
 270 approximated to

$$v_s \approx \frac{\partial u}{\partial t} = \dot{a}r + \frac{\dot{b}}{r^2}, \quad (15)$$

271 where \dot{a} and \dot{b} are the time derivative of the variables a and b . Direct calculation of \dot{a} and \dot{b} ,
 272 shown in Appendix, leads to expressions which violate the kinematic boundary conditions,

273 i.e. $v_s(r = R_1) \neq U_1$ and $v_s(r = R_2) \neq U_2$, where we define $U_1 = \dot{R}_1$ and $U_2 = \dot{R}_2$.
274 However, the deviations from the kinematic boundary conditions remain of order $|R_i -$
275 $R_{ie}|/R_{ie}$, consistently with the assumption of small deformation and linear elastic behavior.
276 Hence, we can restrict the velocity to its leading order expression, where R_{1e} coincides with
277 R_1 and R_{2e} with R_2 . This leads to an expression for v_s that can otherwise be obtained
278 directly from Eq. (15) by applying continuity condition at R_1 and R_2 :

$$v_s(r, t) \approx a_v r + \frac{b_v}{r^2}, \quad (16)$$

279 where

$$a_v = \frac{R_2^2(t)U_2 - R_1^2(t)U_1}{R_2^3(t) - R_1^3(t)}, \quad (17)$$

280 and

$$b_v = \frac{[R_2(t)U_1 - R_1(t)U_2]R_1^2(t)R_2^2(t)}{R_2^3(t) - R_1^3(t)}. \quad (18)$$

281 The above calculated displacement and velocity generalize the ones found in [Church](#)
282 (1995) where an incompressible solid material is considered. Such materials are characterised
283 by a traceless deformation tensor:

$$\epsilon_{rr} + \epsilon_{\theta\theta} + \epsilon_{\phi\phi} = 3a = 0, \quad (19)$$

284 leading to the following displacement in the solid:

$$u^{\text{inc}}(r, t) = \frac{R_1^2(t)[R_1(t) - R_{1e}]}{r^2}, \quad (20)$$

285 where we have also used the relation $a = 0$ to reformulate the expression of b . The velocity
 286 v_s given by Eq. (16) then becomes:

$$v_s^{\text{inc}}(r, t) = \frac{R_1^2(t)U_1}{r^2}. \quad (21)$$

287 Eqs. (20) and (21) are identical to the ones found in Church (1995) where the solid velocity
 288 was calculated directly from the law conservation of the mass for an incompressible fluid
 289 $\nabla \cdot \mathbf{v}_s = 0$, while the displacement was deduced from volume conservation that reads, in the
 290 small deformation limit, $\nabla \cdot \mathbf{u} = 0$. Note that the two approaches are cross-consistent only
 291 in the small deformation framework: then in this case $\nabla \cdot \mathbf{u} = 0$, and moreover the $1/r^2$
 292 behaviour of v_s is recovered only if Eq. (14) is approximated to Eq. (15).

293 Note finally that the displacement can also be defined on the reference configuration i.e.
 294 using Lagrangian formalism without significant difference (Altenbach *et al.*, 2008).

295 C. Equations of motion in the liquid

296 The conservation of mass for an incompressible fluid in a spherical coordinate system
 297 gives:

$$\frac{1}{r^2} \frac{\partial}{\partial r}(r^2 \mathbf{v}) = 0, \quad (22)$$

298 where $\mathbf{v} = (v_f(r), 0, 0)$ is the radial Eulerian velocity vector in the fluid. For $r = R_2$,
 299 $v_f(r = R_2) \equiv U_2$.

300 The velocity profile of the fluid is then:

$$v_f(r) = \frac{U_2 R_2^2}{r^2}. \quad (23)$$

301 The Navier-Stokes equation for an incompressible fluid and irrotational flow writes (Lan-
 302 dau and Lifschitz, 1987):

$$\rho_f \left(\frac{\partial v_f}{\partial t} + v_f \frac{\partial v_f}{\partial r} \right) = -\frac{\partial P}{\partial r}. \quad (24)$$

303 Integration of Eq. (24) between R_2 and $+\infty$, using Eq. (23), leads to:

$$\rho_f \left(R_2 \dot{U}_2 + \frac{3}{2} U_2^2 \right) = P_{f|r=R_2} - P_\infty, \quad (25)$$

304 where $P_{f|r=R_2}$ is the pressure in the fluid near the shell boundary, and P_∞ is the sum of the
 305 applied acoustic pressure $P_{ac}(t)$ and the ambient pressure P_0 .

306 In addition, conservation of radial momentum at the external surfaces of the shell imposes:

307

$$-P_G(t) = (\sigma_{rr}^{el} + \sigma_{rr}^{visc})|_{r=R_1} - \frac{2\gamma_1}{R_1}, \quad (26)$$

308 and:

$$(\sigma_{rr}^{el} + \sigma_{rr}^{visc})|_{r=R_2} = -P_f|_{r=R_2} + \sigma_{rr}^f|_{r=R_2} - \frac{2\gamma_2}{R_2}, \quad (27)$$

309 where γ_1 and γ_2 are the surface tensions respectively at the internal and external boundaries
 310 of the shell, and $P_G(t)$ is the pressure of the gas inside the bubble. We assume the gas
 311 to obey a polytropic law, such that $P_G(t) = P_{g0} (R_{10}/R_1)^{3\kappa}$, where P_{G0} is the equilibrium
 312 gas pressure and κ is the polytropic exponent of the gas. The radial component σ_{rr}^f of the
 313 viscous stress equals:

$$\sigma_{rr}^f = 2\mu_f \frac{\partial v_f}{\partial r} = -4\mu_f \frac{U_2 R_2^2(t)}{r^3}. \quad (28)$$

314 The normal stresses in the shell are obtained from Eqs. (5), (6), (11) and (15), noting
 315 that as done for the velocity, the strain rate $\dot{\epsilon}$ is approximated in the linear elasticity limit

316 to: $\dot{\epsilon} = \partial\epsilon/\partial t$, therefore the relation between $\dot{\epsilon}$ and v_s is similar to that between ϵ and u .

317 We have then:

$$\sigma_{rr}^{el} = 3K'a - 4G'\frac{b}{r^3}, \quad (29)$$

$$\sigma_{rr}^{visc} = 3\mu_K a_v - 4\mu_G \frac{b_v}{r^3}. \quad (30)$$

318 Inserting (29) and (30) in the first boundary condition (26) leads to a first equation for

319 R_1 and R_2 :

$$-P_G + 2\frac{\gamma_1}{R_1} = 3K'a - 4G'\frac{b}{R_1^3} + 3\mu_K a_v - 4\mu_G \frac{b_v}{R_1^3}. \quad (31)$$

320 Replacing a , b , a_v and b_v by their values (12), (13), (17) and (18) in the above equation,

321 one eventually gets:

$$\begin{aligned} -P_G + 2\frac{\gamma_1}{R_1} &= 3K' \frac{R_2^2(R_2 - R_{2e}) - R_1^2(R_1 - R_{1e})}{R_2^3 - R_1^3} \\ &- 4G' \frac{[R_2(R_1 - R_{1e}) - R_1(R_2 - R_{2e})]R_2^2}{(R_2^3 - R_1^3)R_1} \\ &+ 3\mu_K \frac{R_2^2 U_2 - R_1^2 U_1}{R_2^3 - R_1^3} - 4\mu_G \frac{(R_2 U_1 - R_1 U_2) R_2^2}{(R_2^3 - R_1^3)R_1}. \end{aligned} \quad (32)$$

We use the second boundary condition (27) to get rid of the unknown fluid pressure in Eq. (25), such that:

$$\begin{aligned} \rho_f \left(R_2 \dot{U}_2 + \frac{3}{2} U_2^2 \right) &= -\frac{2\gamma_2}{R_2} - P_\infty - 4\mu_f \frac{U_2}{R_2} \\ &- 3K'a + 4G'\frac{b}{R_2^3} - 3\mu_K a_v + 4\mu_G \frac{b_v}{R_2^3}. \end{aligned} \quad (33)$$

322 This equation can be rewritten in a form that resembles a Rayleigh-Plesset equations by
 323 replacing the term $R_2 - R_{2e}$ in a and b thanks to Eq. (32) :

$$\begin{aligned}
 & \rho_f \left(R_2 \dot{U}_2 + \frac{3}{2} U_2^2 \right) = -P_0 - P_{ac}(t) - 2 \frac{\gamma_2}{R_2} - 4 \mu_f \frac{U_2}{R_2} \\
 & + \left(P_G - 2 \frac{\gamma_1}{R_1} \right) \left(1 - \frac{4G'}{3K' + 4G'} \frac{R_2^3 - R_1^3}{R_2^3} \right) \\
 & - 4G' \frac{3K'}{3K' + 4G'} \frac{R_2^3 - R_1^3}{R_2^3} \frac{R_1 - R_{1e}}{R_1} \\
 & + 4 \frac{U_2}{R_2} \left[\mu_G \left(1 - \frac{4G'}{3K' + 4G'} \right) - \mu_K \frac{3G'}{3K' + 4G'} \right] \\
 & - 4 \frac{U_1}{R_1} \left[\mu_G \left(1 - \frac{4G'}{3K' + 4G'} \right) - \mu_K \frac{3G'}{3K' + 4G'} \frac{R_1^3}{R_2^3} \right].
 \end{aligned} \tag{34}$$

324 In this expression, it is interesting to observe that the elastic contribution of the internal
 325 gas is modulated by the intrinsic elastic properties of the shell. This feature will disappear
 326 in the incompressible limit. Eq. (32) and Eq. (34) constitute a system of differential
 327 equations for the two unknowns R_1 and R_2 . For incompressible materials, the Rayleigh-
 328 Plesset equation is sufficient as R_1 and R_2 are simply linked through the incompressibility
 329 condition.

330 D. Unstrained Vs Initial Radii

331 As mentioned before, the unstrained radii may be different from the initial radii: $R_{ie} \neq$
 332 R_{i0} . The radius R_{ie} is defined by the unstrained state of the shell before it is plunged into
 333 the liquid, after what stresses within the shell take place, due to the surface tension at the
 334 interfaces, and the internal and external pressures.

335 Taking Eqs. (32) and (34) at equilibrium ($U_1 = U_2 = 0$, $P_\infty = P_0$), one can extract the
 336 displacements $R_{i0} - R_{ie}$. They can be written $R_{1e} = R_{10}(1 + Z_1)$ and $R_{2e} = R_{20}(1 + Z_2)$,

337 with:

$$\begin{aligned}
Z_1 = \frac{1}{3K'} \left[\frac{R_{20}^3}{\hat{V}_S} \left(P_0 + \frac{2\gamma_2}{R_{20}} \right) - \frac{R_{10}^3}{\hat{V}_S} \left(P_{G_0} - \frac{2\gamma_1}{R_{10}} \right) \right] \\
\frac{1}{4G'} \left[\frac{R_{20}^3}{\hat{V}_S} \left(P_0 - P_{G_0} + \frac{2\gamma_2}{R_{20}} + \frac{2\gamma_1}{R_{10}} \right) \right], \tag{35}
\end{aligned}$$

$$\begin{aligned}
Z_2 = \frac{1}{3K'} \left[\frac{R_{20}^3}{\hat{V}_S} \left(P_0 + \frac{2\gamma_2}{R_{20}} \right) - \frac{R_{10}^3}{\hat{V}_S} \left(P_{G_0} - \frac{2\gamma_1}{R_{10}} \right) \right] \\
\frac{1}{4G'} \left[\frac{R_{10}^3}{\hat{V}_S} \left(P_0 - P_{G_0} + \frac{2\gamma_2}{R_{20}} + \frac{2\gamma_1}{R_{10}} \right) \right], \tag{36}
\end{aligned}$$

338 where $\hat{V}_S = R_{20}^3 - R_{10}^3$.

339 These formulations highlight the effect of compressibility, which is the same for the two
340 radii.

341 If the shell is incompressible ($K' \gg P_{G_0}, P_0, \gamma_i/R_{10}$), one has:

$$Z_i^{inc} = \left(P_0 - P_{G_0} + \frac{2\gamma_1}{R_{10}} + \frac{2\gamma_2}{R_{20}} \right) \frac{R_{20}^3 + R_{10}^3 - R_{i0}^3}{4G'\hat{V}_S}, \tag{37}$$

342 which is identical to the expression found in (Church, 1995) when $P_{G_0} = P_0$, which was
343 hypothesized in that paper.

344 In Doinikov and Dayton (2006), where incompressible shells are also considered, the
345 authors find the same relation as Eq. (37), which is the first order of their Eq. (33).
346 However in a second step they go further in the calculation using deformation profiles that
347 are valid in the compressible case and find expressions (Eqs. (40) and (41) in their paper)
348 that contradicts our findings, and the ones in Church (1995) and in Sarkar *et al.* (2005)
349 in that they find the counter-intuitive result that surface tension tends to increase the
350 equilibrium radius. Here, we are satisfied with the observation that an increase of surface

351 tension leads to a shrinkage of the shell. This altogether suggests that care must be taken
 352 not to mix expressions from the compressible case with expressions from the incompressible
 353 case.

354 It is worth emphasizing that in the incompressible case, the ratio of the volume in the
 355 unstressed configuration to that after the shell is plunged in the fluid, namely $[R_{20}^3(1 +$
 356 $Z_2^{inc})^3 - R_{10}^3(1 + Z_1^{inc})^3]/(R_{20}^3 - R_{10}^3)$, is equal to 1 in this model or in the other models
 357 (Church, 1995; Doinikov and Dayton, 2006; Khismatullin and Nadim, 2002) only to first
 358 order in Z_i^{inc} . This corresponds to the domain of validity of the linear elasticity framework.
 359 In the general case, one must therefore restrict the obtained expressions to the first order in
 360 Z_i for consistency.

361 E. Linear analysis

362 Assuming a small-amplitude oscillation, linear equations for the R_i can be obtained using
 363 the following relations:

$$\begin{aligned}
 R_1(t) &= R_{10}[1 + x(t)], \quad |x(t)| \ll 1; \\
 R_2(t) &= R_{20}[1 + y(t)], \quad |y(t)| \ll 1; \\
 U_1(t) &= R_{10}\dot{x}; \\
 U_2(t) &= R_{20}\dot{y};
 \end{aligned}
 \tag{38}$$

364 To the first order in x , y , Z_1 and Z_2 , Eq. (32) becomes, after using Eqs (35) and (36):

$$\begin{aligned}
& - \left(3\kappa P_{G_0} - \frac{2\gamma_1}{R_{10}} + \frac{4G'R_{20}^3 + 3K'R_{10}^3}{R_{20}^3 - R_{10}^3} \right) x \\
& + \frac{(4G' + 3K')R_{20}^3}{R_{20}^3 - R_{10}^3} y - \frac{4\mu_G R_{20}^3 + 3\mu_K R_{10}^3}{R_{20}^3 - R_{10}^3} \dot{x} \\
& + \frac{(4\mu_G + 3\mu_K)R_{20}^3}{R_{20}^3 - R_{10}^3} \dot{y} = 0.
\end{aligned} \tag{39}$$

365 Dividing this equation by K' and taking the limit $K' \rightarrow \infty$, one gets $x = yR_{20}^3/R_{10}^3$, which
366 is the relationship obtained for an incompressible material as in Church (1995). Eq. (39)
367 is therefore a generalization of this relationship for the case of a viscoelastic compressible
368 material.

369 Eq. (39) together with the linearized Rayleigh-Plesset-like equation obtained from Eq.
370 (34) constitutes the following linear system:

$$M\ddot{X} + B\dot{X} + KX = F(t), \tag{40}$$

371 where:

$$\begin{aligned}
X &= \begin{pmatrix} x \\ y \end{pmatrix}, F(t) = \begin{pmatrix} -P_{ac}(t) \\ 0 \end{pmatrix}, M = \begin{bmatrix} 0 & \rho_f R_{20}^2 \\ 0 & 0 \end{bmatrix} \\
B &= \begin{bmatrix} b_{11} & b_{12} \\ \frac{-4\mu_G R_{20}^3 - 3\mu_K R_{10}^3}{R_{20}^3 - R_{10}^3} & \frac{(4\mu_G + 3\mu_K)R_{20}^3}{R_{20}^3 - R_{10}^3} \end{bmatrix}
\end{aligned} \tag{41}$$

372

$$\text{with } b_{11} = 12 \frac{K'\mu_G - G'\mu_K \frac{R_{10}^3}{R_{20}^3}}{3K' + 4G'},$$

373

$$b_{12} = 4 \left(\mu_f + 3 \frac{K'\mu_G - G'\mu_K}{3K' + 4G'} \right),$$

374 and

$$K = \begin{bmatrix} k_{11} & \frac{-2\gamma_2}{R_{20}} \\ k_{21} & \frac{(4G'+3K')R_{20}^3}{R_{20}^3-R_{10}^3} \end{bmatrix} \quad (42)$$

375 with

$$k_{11} = \left(3\kappa P_{G_0} - \frac{2\gamma_1}{R_{10}} \right) \left(1 - \frac{4G'}{3K'+4G'} \frac{R_{20}^3 - R_{10}^3}{R_{20}^3} \right) + \frac{12G'K'}{3K'+4G'} \frac{R_{20}^3 - R_{10}^3}{R_{20}^3},$$

376

$$k_{21} = -3\kappa P_{G_0} + \frac{2\gamma_1}{R_{10}} - \frac{4G'R_{20}^3 + 3K'R_{10}^3}{R_{20}^3 - R_{10}^3}.$$

377 The free oscillations of the shells ($P_{ac} = 0$) are described by non-trivial harmonic solutions
 378 of the above system $X = X_0 e^{\lambda t}$, where $\lambda = -\delta + i\omega$, that are obtained by setting $\det(\lambda^2 M +$
 379 $\lambda B + K) = 0$. This leads to a polynomial equation of order 3 for λ , which can be solved
 380 analytically (yet leading to very long expressions) or numerically. This equation reads

$$c_1 \lambda^3 + c_2 \lambda^2 + c_3 \lambda + c_4 = 0, \quad (43)$$

where

$$c_1 = -b_{21}m_{12}, \quad c_2 = \det[B] - k_{21}m_{12}, \quad (44)$$

$$c_3 = b_{11}k_{22} - b_{12}k_{21} - b_{21}k_{12} + b_{22}k_{11}, \quad c_4 = \det[K].$$

381 For sake of comparison with the literature, and making use of the observation that damp-
 382 ing coefficient is usually small, we present the leading order approximation and the first-order
 383 correction with respect to this damping coefficient in the following. Note that this is a sec-

384 ond and independent approximation, based on the usual values of dissipation factors, that
 385 is added to that of small deformation.

386 F. Leading order approximation

387 For $B = 0$, Eq. (43) becomes $\det[K] - k_{21}m_{12}\lambda^2 = 0$, therefore $\lambda = i\omega_0$ where the
 388 undamped resonance frequency ω_0 is given by:

$$\omega_0^2 = \frac{3K' + 4G'}{\rho_f R_{20}^2} \left[4G' \frac{3K'}{3K' + 4G'} \frac{R_{20}^3 - R_{10}^3}{R_{20}^3} + \left(3\kappa P_{G0} - \frac{2\gamma_1}{R_{10}} \right) \left(1 - \frac{4G'}{3K' + 4G'} \frac{R_{20}^3 - R_{10}^3}{R_{20}^3} \right) \right] \\ \times \left[\left(3\kappa P_{G0} - \frac{2\gamma_1}{R_{10}} \right) \frac{R_{20}^3 - R_{10}^3}{R_{20}^3} + 4G' + 3K' \frac{R_{10}^3}{R_{20}^3} \right]^{-1} - \frac{2\gamma_2}{\rho_f R_{20}^3}. \quad (45)$$

389 This constitutes the central result of this paper. The last term in the above expression is
 390 the classical contribution of the surface tension of the outer surface, which acts against an
 391 effective mass of fluid whose scale is given by the shell size. By contrast, the contribution
 392 of the shell elasticity and of the elastic forces (acting on the inner side of the shell (the gas
 393 pressure and the surface tension) are strongly coupled. As discussed later on, this coupling
 394 disappears in the incompressibility limit. As in the Rayleigh-Plesset expression for a free
 395 bubble — $\omega_0^{RP} = \left[\frac{1}{\rho_f R_{20}^2} \left(3\kappa P_{G0} - \frac{2\gamma_1}{R_{20}} - \frac{2\gamma_2}{R_{20}} \right) \right]^{1/2}$, that is recovered here with Eq. (45) taken
 396 in the limit of vanishing shell volume ($R_{10} \rightarrow R_{20}$) — adding surface tension makes the shell
 397 pulsation decrease, at *fixed* P_{G0} . In practice, P_{G0} is not known nor measurable and it would
 398 be preferable to express the pulsation as a function of the external pressure P_0 . While this
 399 is easily done for a free bubble, leading to an increase of pulsation with surface tensions,
 400 this is more complex in the present situation: P_{G0} and P_0 also couple through the elastic

401 stress within the shell, which depends on the reference configuration (R_{1e}, R_{2e}) , which is not
 402 known in general.

403 In this context, measuring oscillation frequency cannot be sufficient to determine the
 404 elastic constants of the shell material. Even if surface tensions are assumed to be zero, and
 405 considering that the external radius is known, we are left with four unknowns which are
 406 the two elastic constants, the internal pressure and the internal radius. This is one more
 407 than in Church model and two more than in zero-thickness shell models. Even in these
 408 simpler model, and in all cases, one needs to know more on the fabrication process of the
 409 shell to know their stress-free state or to make additional assumptions. In Church (1995),
 410 it is for instance assumed that permeability of the shell under study allows to consider that
 411 $P_{G0} = P_0$, which may be true for thin lipid shells, but not for thicker shells, as pointed out
 412 in Doinikov and Dayton (2006).

413 For an incompressible shell, the undamped natural frequency becomes:

$$\begin{aligned} \omega_0^{inc} = & (\rho_S R_{10}^2 \alpha^{inc})^{-1/2} \left(3\kappa P_{G0} - \frac{2\gamma_1}{R_{10}} - \frac{2\gamma_2}{R_{20}} \frac{R_{10}^3}{R_{20}^3} \right. \\ & \left. + 4G' \frac{R_{20}^3 - R_{10}^3}{R_{20}^3} \right)^{1/2}, \text{ with } \alpha^{inc} = \frac{\rho_f R_{10}}{\rho_S R_{20}}. \end{aligned} \quad (46)$$

414 This differs from the expression proposed in Church (1995):

$$\begin{aligned} \omega_0^{Ch} = & (\rho_S R_{10}^2 \alpha^{Ch})^{-1/2} \left\{ 3\kappa P_{G0} - \frac{2\gamma_1}{R_{10}} - \frac{2\gamma_2}{R_{20}} \frac{R_{10}^3}{R_{20}^3} \right. \\ & \left. + 4G' \frac{R_{20}^3 - R_{10}^3}{R_{20}^3} \left[1 + Z_1^{Ch} \left(1 + \frac{3R_{10}^3}{R_{20}^3} \right) \right] \right\}^{1/2}, \end{aligned} \quad (47)$$

415 with

$$\alpha^{Ch} = \frac{\rho_f R_{10}}{\rho_S R_{20}} + 1 - \frac{R_{10}}{R_{20}}. \quad (48)$$

416 A first difference lies in the effective mass characterized by the coefficient α , since we
 417 neglected the inertia of the shell. Note that it introduces a correction on ω_0^2 of order d_0/R_{20} ,
 418 where $d_0 = R_{20} - R_{10}$, that is of at most a few percent for actual UCAs.

419 The other difference lies in the presence of a Z_1^{Ch} term in Church (1995). This is due
 420 to a subtle inconsistency in the linearizing process: as discussed in Sec. VD, Z_1^{Ch} must be
 421 considered as a small parameter in order to keep the validity of linear elasticity framework. It
 422 characterizes the difference between the unstrained state and the equilibrium state, the same
 423 way as x and y in Eq. 38 characterize the difference between the actual and the equilibrium
 424 state. Terms like xZ_1 should therefore not be included in the linearized equation, contrary
 425 to what is done in Church (1995) between his Eqs. (12) and (17). Replacing Z_1^{Ch} by its
 426 value in ω_0^{Ch} one gets:

$$\omega_0^{Ch} = (\rho_S R_{10}^2 \alpha^{Ch})^{-1/2} \left[3\kappa P_{G0} + \frac{2\gamma_1}{R_{10}} \frac{3R_{10}^3}{R_{20}^3} + \frac{2\gamma_2}{R_{20}} \left(1 + \frac{2R_{10}^3}{R_{20}^3} \right) + 4G' \left(\frac{R_{20}^3 - R_{10}^3}{R_{20}^3} \right) \right]^{1/2}. \quad (49)$$

427 One can see that the contributions of the surface tension are incorrectly estimated with
 428 this contested expression by Church, as this expression does not converge to the Rayleigh-
 429 Plesset pulsation ω_0^{RP} in the vanishing volume limit.

430 G. First order approximation

431 If Eq. (43) is expanded to the first orders in b_{ij} and δ , one gets that $\omega = \omega_0$ and

$$\delta = -\frac{c_3 + b_{21}m_{12}\omega_0^2}{2k_{21}m_{12}}, \quad (50)$$

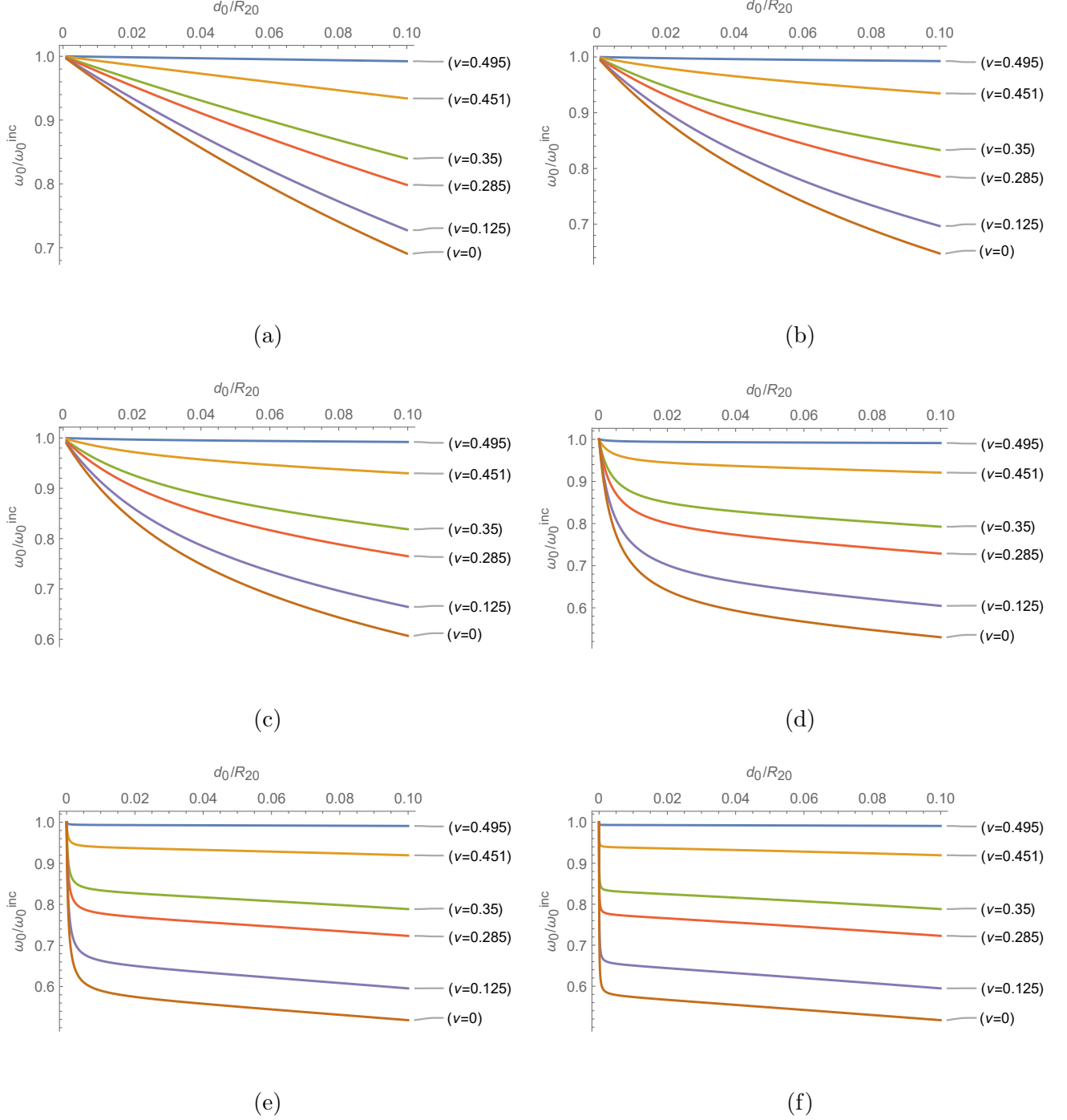


FIG. 1. Ratio of the undamped resonance frequencies ω_0/ω_0^{inc} as a function of d_0/R_{20} , in the absence of external surface tension. G' is fixed to **a)** $G' = \tilde{P}$, **b)** $G' = 5\tilde{P}$, **c)** $G' = 10\tilde{P}$, **d)** $G' = 100\tilde{P}$, **e)** $G' = 1000\tilde{P}$, **f)** $G' = 10^4\tilde{P}$. \tilde{P} is $P_{G_0} - \frac{2\gamma_1}{3\kappa R_{10}}$. We varied K' as $100G'$, $10G'$, $3G'$, $2G'$, G' and $\frac{2}{3}G'$, and the corresponding Poisson ratios $\nu = (3K' - 2G')/(6K' + 2G')$ are shown on each curve. Note that when $\nu = -1$, $\omega_0 \approx 0$.

432 which can be reformulated as:

$$\delta = \frac{1}{2m_{12}} \left[b_{12} - b_{11} \frac{k_{22}}{k_{21}} + \frac{k_{11}}{k_{21}^2} (b_{21}k_{22} - b_{22}k_{21}) \right]. \quad (51)$$

433 As seen in Eq. (40), the first term b_{12} in the above expression represents the damping
 434 directly affecting the motion of the external radius of the shell, through the fluid viscosity
 435 and a contribution of the shell viscosity. The second term stems from the damping affecting
 436 the motion of the internal radius, which is weighted by the elastic contribution k_{22}/k_{21} . The
 437 third term stems from the coupling between dissipation and elastic deformation inside the
 438 shell.

439 For an incompressible shell, the damping ratio δ in Eq. (50) simply becomes:

$$\delta^{inc} = 2 \frac{(R_{20}^3 - R_{10}^3)\mu_G + R_{10}^3\mu_f}{\rho_S R_{10}^2 R_{20}^3 \alpha^{inc}}. \quad (52)$$

440 In Church (1995) it reads:

$$\delta^{Ch} = 2 \frac{(R_{20}^3 - R_{10}^3)\mu_G + R_{10}^3\mu_f}{\rho_S R_{10}^2 R_{20}^3 \alpha^{Ch}}. \quad (53)$$

441 As for the pulsation a difference of a few percents remains, which is related to the absence
 442 of shell mass in our model.

443 H. Discussion: effect of compressibility on ω_0

444 We discuss in this section to which extent the frequency is modified when the material
 445 is compressible. We first consider a reference configuration, denoted \mathcal{R} , which is considered
 446 in (Church, 1995): $d_0 = 15$ nm, $P_{G_0} = 101.3$ kPa, $\rho_f = 1000$ kg/m³, $\rho_S = 1100$ kg/m³,

447 $\mu_f = 0.001$ Pa.s, $G' = 88.8$ MPa, $\gamma_1 = 0.04$ N/m, $\gamma_2 = 0.005$ N/m and $\kappa = 7/5$. For such a
448 shell whose external radius lies in the range $1 - 10 \mu\text{m}$, we find that $0.99 < \omega_0^{inc}/\omega_0^{Ch} < 1$,
449 which indicates that while our model has led us to neglect the inertia of the shell, this
450 assumption will modify the final result by a negligible amount. Note that in this exam-
451 ple, since $\gamma_i/R_{i0} \ll G'$, the inaccuracy that we exhibited in the Church (1995) model has
452 no quantitative consequence. In the following, we consider ω_0^{inc} as the reference value for
453 discussion.

454 We now discuss the effect of compressibility together with an evaluation on the impact
455 of the contribution of gas compressibility. For most commercial shells, G' is actually 10 to
456 1000 times the ambient pressure (see e.g. Table III). Since the G' contribution is weighted
457 by d/R (which is roughly the ratio of the shell material volume over the volume of gas),
458 both contributions are likely to contribute with comparable weight.

459 As the contribution of the external surface tension is purely additive, for simplicity we set
460 $\gamma_2 = 0$ and consider several values of $\tilde{P} = P_{G_0} - \frac{2\gamma_1}{3\kappa R_{10}}$, that characterizes the contribution of
461 the inner gas to UCA oscillations. In this case, regarding space variables, $R_{20} \times \omega_0$ depends
462 only on d_0/R_{20} .

463 In Fig. 1, the ratio ω_0/ω_0^{inc} is calculated for different values of G' and K' , that are set
464 relatively to \tilde{P} .

465 The influence of compressibility is significant: it reduces the resonance frequency, all
466 the more that the relative thickness d_0/R_{20} increases, the Poisson ratio decreases, and the
467 shear modulus increases. In particular, when the bubble radius decreases at fixed thickness,
468 this effect of compressibility will become relatively more important. Compressibility thus

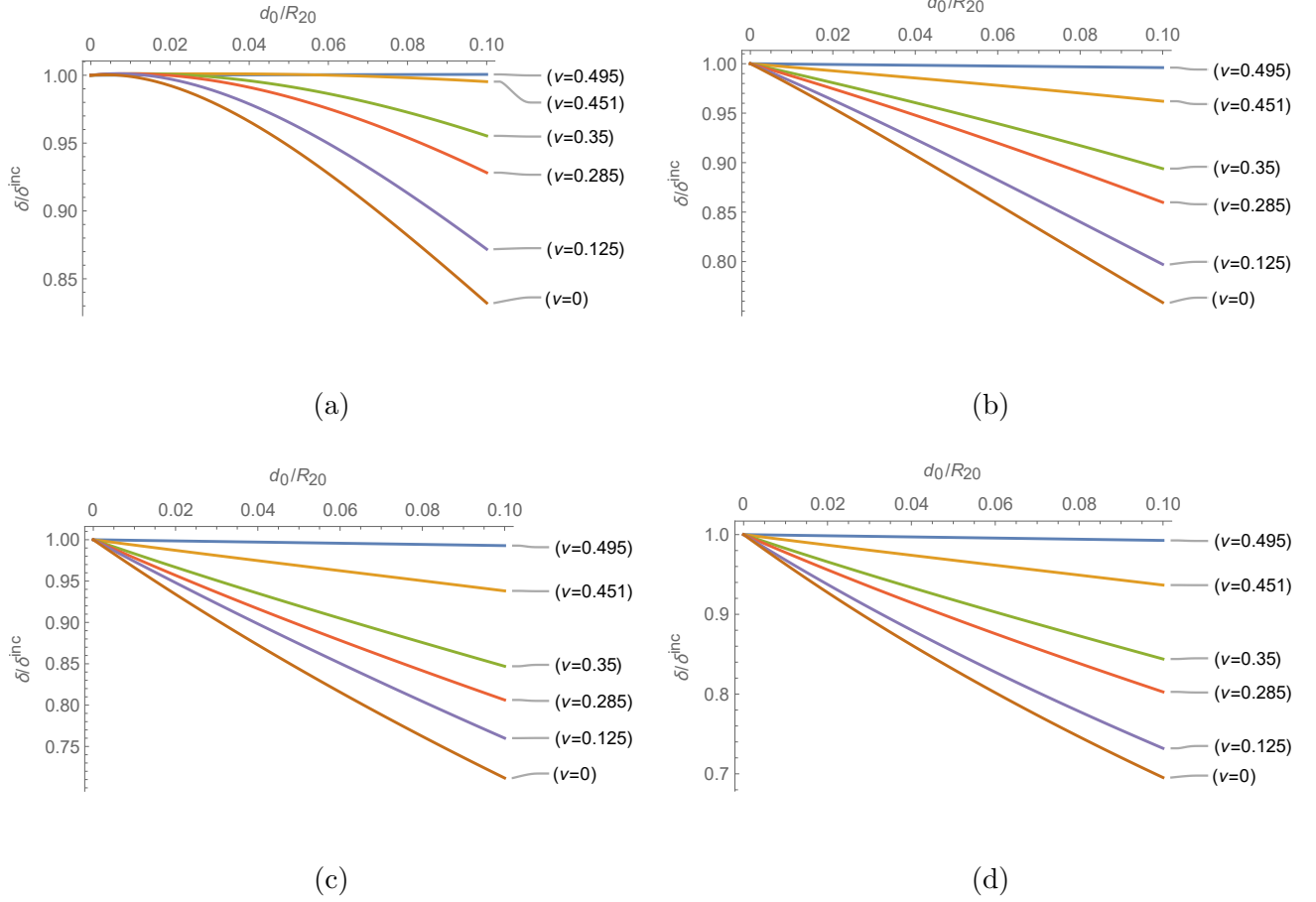


FIG. 2. Ratio of the damping ratios δ/δ^{inc} as a function of d_0/R_{20} , in the absence of external surface tension. G' is fixed to **a)** $G' = \tilde{P}$, **b)** $G' = 1.5\tilde{P}$, **c)** $G' = 4\tilde{P}$, **d)** $G' = 5\tilde{P}$. \tilde{P} is $P_{G_0} - \frac{2\gamma_1}{3\kappa R_{10}}$. We varied K' as $100G'$, $10G'$, $3G'$, $2G'$, G' and $\frac{2}{3}G'$, and the corresponding Poisson ratios $\nu = (3K' - 2G')/(6K' + 2G') = (3\mu_K - 2\mu_G)/(6\mu_K + 2\mu_G)$ are shown on each curve. Note that curves do not vary by more than 1% for $G' \geq 5\tilde{P}$.

469 introduces a dependency of the frequency on the shell radius that is more complex than in
 470 the incompressible case, where $\omega_0 \propto 1/R_{20}$ in the thin shell limit.

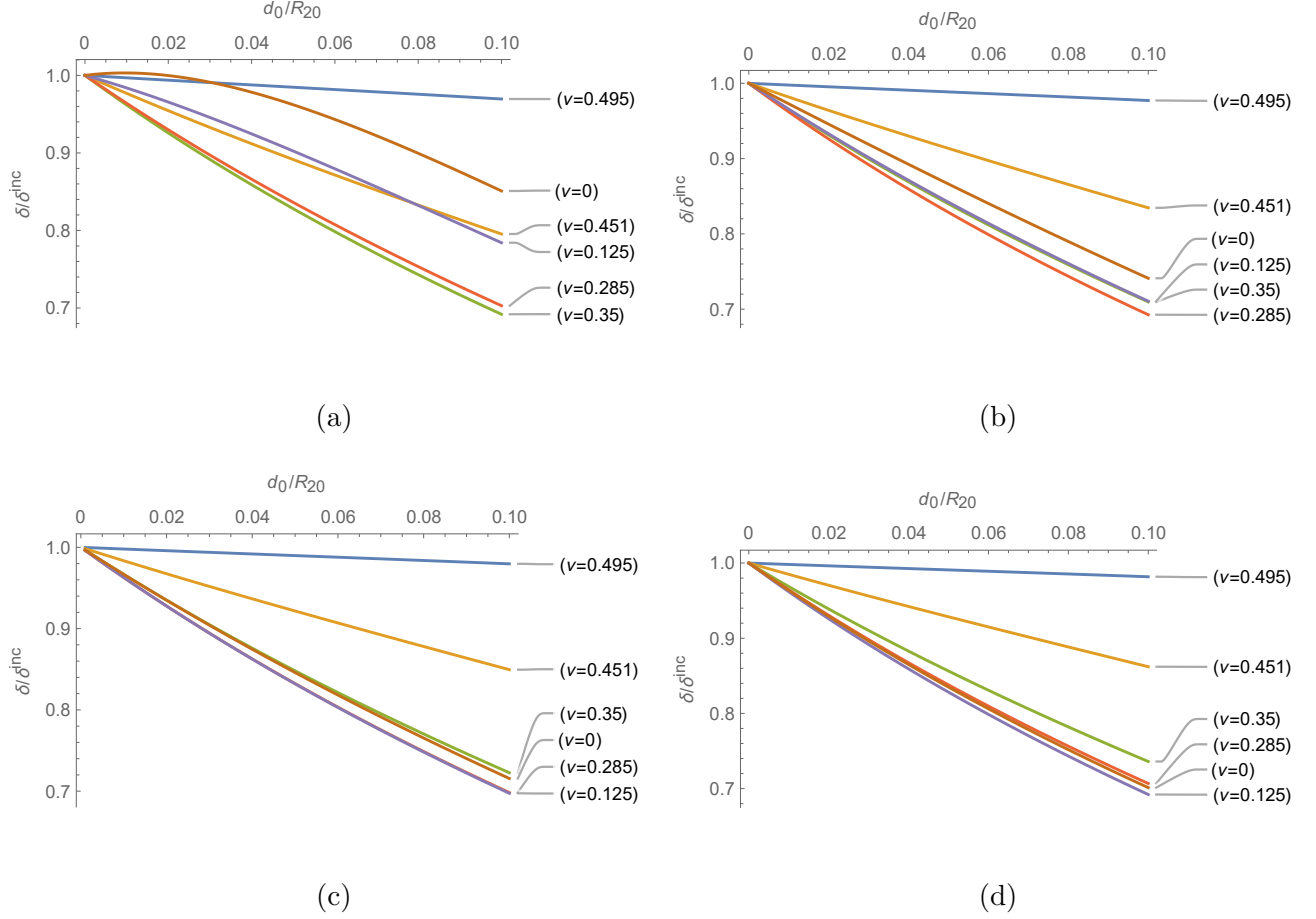


FIG. 3. Ratio of the damping ratios δ/δ^{inc} as a function of d_0/R_{20} , in the absence of external surface tension. G' is fixed to a) $G' = \tilde{P}$, b) $G' = 2\tilde{P}$, c) $G' = 3\tilde{P}$, d) $G' = 5\tilde{P}$. \tilde{P} is $P_{G_0} - \frac{2\gamma_1}{3\kappa R_{10}}$. We varied K' as $100G'$, $10G'$, $3G'$, $2G'$, G' and $\frac{2}{3}G'$, and the corresponding Poisson ratios $\nu = (3K' - 2G')/(6K' + 2G')$ are shown on each curve. Note that curves do not vary by more than 1% for $G' \geq 5\tilde{P}$. In all cases, $\mu_K = 0.7\mu_G$, following (Pritz, 2009).

471 For large values of G' , Eq. (45) yields, after setting $K' = \frac{2(1+\nu)}{3(1-2\nu)}G' \equiv f(\nu)G'$,

$$\omega_{0,G' \gg \hat{P}}^2 = \frac{1}{\rho_f R_{20}^2} \left(4G' \frac{R_{20}^3 - R_{10}^3}{R_{20}^3} \right) \frac{3f(\nu)}{4 + 3f(\nu) \frac{R_{10}^3}{R_{20}^3}}. \quad (54)$$

472 Then,

$$\left(\frac{\omega_{0,G' \gg \hat{P}}}{\omega_{0,G' \gg \hat{P}}^{inc}}\right)^2 = \frac{3f(\nu)(1 - \frac{d_0}{R_{20}})^3}{4 + 3f(\nu)(1 - \frac{d_0}{R_{20}})^3} \equiv g(\nu, d_0, R_{20}). \quad (55)$$

473 In the thin shell limit, compressibility leads to a decrease of the pulsation squared by a
474 factor $\sqrt{f(\nu)/[f(\nu) + 4/3]}$.

475 Eq. (54) can also be interpreted from the following practical viewpoint: if one measures
476 a shell pulsation and deduces from this measurement a value G'_0 for the shell, assuming
477 incompressibility, the same measurement can also be obtained with a shell of shear modulus
478 G' and Poisson ratio ν obeying $G'_0 = G'g(\nu, d_0, R_{20})$.

479 The consequences are two-fold: as $g(\nu, d_0, R_{20})$ is significantly smaller than 1 as soon as
480 $\nu < 1/2$, the existence of unforeseen compressibility will lead to an underestimation of the
481 shear modulus. For instance, for a shell of estimated thickness 15 nm and external radius 2
482 μm , if ν happens to be 0.4 instead of 0.5, $g(\nu, d_0, R_{20}) = 0.77$, which means that the shear
483 modulus will be underestimated by 23%. This value reaches 28% if $d_0 = 200$ nm.

484 Second, as g is an increasing function of R_{20} , using a model for incompressible material
485 can lead to an artificial increase of the (apparent) shear modulus with the radius, a feature
486 regularly pointed out in the literature.

487 These compressibility effects are more pronounced for thick shells, and we are not aware
488 of oscillation measurements in the literature based on thick shells like polymeric shells. In
489 addition, a more quantitative analysis of the impact of compressibility on the radius de-
490 pendency of the frequency, by comparison with other suggestions like non-linear effects,
491 requires to know more about the inner pressure inside the considered shells, which depends
492 on their manufacturing process and also potentially on the allotted time for pressure equal-

493 ization through transmembrane diffusion. This point becomes even more evident in the
 494 zero-thickness shell limit that is discussed in the following.

495 I. Discussion: from finite thickness to zero-thickness shell

496 For vanishing thickness, considering the corresponding limit in our finite thickness model
 497 or in that of Church (1995) leads to models that can be compared to zero-thickness models.
 498 In particular, in Hoff *et al.* (2000), the vanishing thickness limit of Church model is considered
 499 and the resulting frequency is shown to be similar with that obtained in de Jong *et al.* (1992)
 500 or in the linearized version of Marmottant *et al.* (2005):

$$\omega_0^{\text{0-thickness}} = (\rho_f R_0^2)^{-1/2} \left(3\kappa P_{G0} + 4 \frac{\chi_0}{R_0} \right)^{1/2}, \quad (56)$$

501 where R_0 is the shell radius and χ_0 has the dimension of a surface tension and includes
 502 in-plane elasticity effects as well as surface tension effects on both sides of the interface
 503 (de Jong *et al.*, 1992; Hoff *et al.*, 2000; Marmottant *et al.*, 2005; Sarkar *et al.*, 2005; van der
 504 Meer *et al.*, 2007). In Hoff *et al.* (2000) when surface tension effects are neglected, χ_0 is
 505 shown to be equal to $\chi_{2D} = 3G'd_0$, the in-plane surface contraction modulus.

506 We examine here the small thickness limit of our model. We consider only the incom-
 507 pressibility limit, which is already an interesting source for discussion and allows direct
 508 comparison with the actual zero-thickness models.

509 Keeping only the 0th and 1st orders in d_0/R_{20} in Eq. (45), we find the following expansion:

$$\omega_0^{inc} = (\rho_f R_{20}^2)^{-1/2} \left[3\kappa P_{G0} - \frac{2\gamma_1}{R_{20}} - \frac{2\gamma_2}{R_{20}} + \left(12G' + 9\kappa P_{G0} - \frac{8\gamma_1}{R_{20}} \right) \frac{d_0}{R_{20}} + o\left(\frac{d_0}{R_{20}}\right) \right]^{1/2}. \quad (57)$$

510 By comparison with Eq. (56), this introduces a correction that implies that pressure and
 511 inner surface tension have a more complex space-dependency than that proposed in the
 512 Church-Hoff model, where the 1st order in d_0/R_{20} was neglected in the inertial term.

513 We attempt to discuss the implication of our modeling regarding the interpretation of
 514 experimental data. Authors generally consider a given experiment for a set of shells of
 515 different sizes, which they either watch (measuring thus the radius oscillation ([Chetty *et al.*, 2008](#);
 516 [Doinikov *et al.*, 2009](#); [Li *et al.*, 2013](#); [Tu *et al.*, 2009](#); [van der Meer *et al.*, 2007](#)))
 517 or listen (measuring thus the acoustic transmission ([Parrales *et al.*, 2014](#))). The obtained
 518 curves are then fitted according to the chosen model, which results in the determination
 519 of the corresponding elastic modulus for each shell radius. It is then generally observed
 520 that this constant increases with the radius, which highlights the limit of the chosen model.
 521 Other parameters are generally considered as known but they are not always given by the
 522 authors. In particular, the inner pressure P_{G0} is sometimes set to atmospheric pressure
 523 with not much justification ([Doinikov *et al.*, 2009](#); [Li *et al.*, 2013](#); [Tu *et al.*, 2009](#); [van der
 524 Meer *et al.*, 2007](#)) but some authors do not specify their choice ([Parrales *et al.*, 2014](#)). On
 525 the other hand, the descriptions of fabrication processes of home-made microshells often
 526 mention initial gaz pressure larger than 1 bar ([Parrales *et al.*, 2014](#); [Segers *et al.*, 2016](#)),
 527 which questions the hypothesis of atmospheric pressure inside the shells. Though diffusion
 528 may favor this hypothesis, such a phenomenon will also induce stresses inside the shell

529 reaching its new equilibrium, resulting in uncertainties on the exact state around which the
530 oscillations take place.

531 Finally, it is generally observed in all papers that while the radius varies by a factor 2 to
532 3, the corresponding elastic modulus varies by a factor 3 to 4. In [Parrales *et al.* \(2014\)](#) this
533 is the case but contrary to most other papers where only the values of the elastic constants
534 are given, the measured frequencies are also mentioned. We therefore use these raw data to
535 make the following comments. In [Fig. 4](#), the pulsations found in the experiments are plotted
536 as a function of shell radius. Those shells are lipidic shells, therefore the small-thickness limit
537 holds. The fit of their data by the usual zero-thickness law ([Eq. 56](#)), assuming $P_{G0} = 1$
538 bar and $\kappa = 1.4$, is not that good, which illustrates the conclusions of the authors who,
539 considering each radius separately, showed that the elastic modulus must be an increasing
540 function of the radius. We note however that the fit yields $\chi_0 = 0.21$ N/m, which is smaller
541 than all the values reported by the author for the different shell radii, which questions
542 the (implicit) choice of inner pressure or of polytropic constant they made. Interestingly,
543 letting P_{G0} free leads to a better fit, with $P_{G0} = 1.6$ bar. This shows the importance of the
544 knowledge of the inner pressure or, equivalently, of the polytropic coefficient that depends
545 on the chosen gas and on the details of the thermodynamics process, as discussed in [Parrales](#)
546 [et al. \(2014\)](#).

547 In the expression for the zero-thickness limit that we established ([Eq. 57](#)), we show
548 that the contribution of pressure is more complex and that it is important to decouple, in
549 the elastic contribution of the interface, bulk effects from surface tension effects: they do
550 not sum up in a simple χ_0 parameter. Using this expression we find an even better fit for

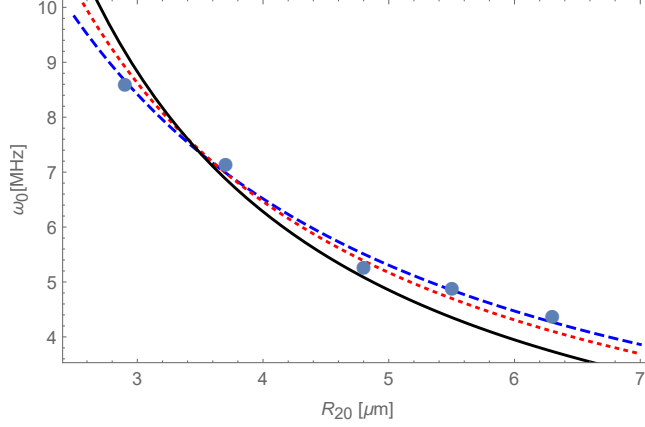


FIG. 4. Dots: experimental pulsations found in [Parrales *et al.* \(2014\)](#) as a function of shell radius. Full black line: fit with Eq. (56) with fixed inner pressure $P_{G0} = 1$ bar and χ_0 as a free parameter. Red dotted line: fit with the same equation but the pressure is also a free parameter. Blue dashed line: fit with Eq. (57) with also the surface tension being a free parameter. Using Eq. (57) allows to recover the full spatial dependency of the data, with a $1/R_0$ and a $1/R_0^{3/2}$ contribution.

551 the data of [Parrales *et al.* \(2014\)](#), illustrating thus the complex interplay between all the
 552 parameters of these models. Note that we do not claim here that the parameters we find
 553 are those that actually characterize the considered shell. Our discussion simply highlights
 554 the need for a good knowledge of a maximum of parameters, if one wishes to extract one
 555 unknown parameter from the sole measurement of oscillation frequencies.

556 J. Discussion: Effect of compressibility on the damping

557 Reminder: our model assumes that $\tau_S = \mu_M/M'$ is much smaller than ω_0^{-1} . In the
 558 following examples, we checked that $\tau_S\omega_0$ is always lower than 0.01. We set here the fluid
 559 viscosity $\mu_f = 0.001$ Pa.s and the shear viscosity $\mu_G = 0.002$ Pa.s.

560 As for the discussion on pulsation, we set $\gamma_2 = 0$ and consider several values of $\tilde{P} =$
561 $P_{G_0} - \frac{2\gamma_1}{3\kappa R_{10}}$. In Fig. 2 we show the ratio of the damping constants δ/δ^{inc} under the hypothesis
562 that μ_K varies with μ_G the same way K' varies with G' that is, the viscous and elastic
563 Poisson ratio are equal (Lemaitre and Chaboche, 1994). In Fig. 3 μ_K is chosen to be equal
564 to $0.7\mu_G$ following Pritz (2009), where it is shown that $2/3 < \mu_K/\mu_G < 1$ for thermodynamic
565 consistency.

566 Compressibility has the effect to make the damping constant decrease. As for the elastic
567 constant determined through the frequency, this may lead to an underestimation of the
568 shear viscosity if an incompressible model is used. For large values of G' and $K' = G'f(\nu)$
569 compared to \tilde{P} , as for the frequencies, the damping depends only on elastic properties
570 through the Poisson ratio, as can be seen through Eqs. (41) and (42) taken in the limit
571 $G', K' \gg \tilde{P}$. In practice, as seen in Figs. 2 and 3, this limit is reached as soon as $G' > 5\tilde{P}$,
572 which is generally the case for actual commercial UCAs. Interestingly, the choice of the
573 model for the viscous Poisson ratio has little impact on the final results: for high values of
574 K', μ_K is not expected to contribute much for both models as its contribution vanishes in
575 the incompressibility limit (see Eq. (52)), and for values of K' comparable G', μ_K is close
576 to μ_G in both models. If the Pritz (2009) model is assumed though, the coupling between
577 elastic and viscous terms is such that the damping is not a monotonous function of the
578 Poisson ratio ν .

579 **VI. TRANSVERSE ISOTROPIC ELASTIC SHELL**

580 We now examine the effect of anisotropy in the properties of a purely elastic material. We
 581 reformulate Eq. (4) using elastic constants corresponding to standard deformations (Itskov
 582 and Aksel, 2002; Lempriere, 1968):

$$\left\{ \begin{array}{l} \sigma_{rr}^{el} = \frac{(1-\nu_{\parallel})E'_r}{1-\nu_{\parallel}-2\frac{E'_{\parallel}}{E'_r}\nu_{\theta r}^2} \epsilon_{rr} + \frac{2\nu_{\theta r}E'_{\parallel}}{1-\nu_{\parallel}-2\frac{E'_{\parallel}}{E'_r}\nu_{\theta r}^2} \epsilon_{\theta\theta} \\ \sigma_{\theta\theta}^{el} = \sigma_{\phi\phi}^{el} = \frac{\nu_{\theta r}E'_{\parallel}}{1-\nu_{\parallel}-2\frac{E'_{\parallel}}{E'_r}\nu_{\theta r}^2} \epsilon_{rr} + \frac{E'_{\parallel}}{1-\nu_{\parallel}-2\frac{E'_{\parallel}}{E'_r}\nu_{\theta r}^2} \epsilon_{\theta\theta} \end{array} \right. , \quad (58)$$

583 where E'_r is the Young modulus for traction in the radial direction while E'_{\parallel} is the Young
 584 modulus in the orthoradial plane. ν_{\parallel} is the Poisson ratio in this same plane, and $\nu_{\theta r}$ the
 585 Poisson ratio governing deformations in the orthoradial plane when there is a radial load ¹.

586 Thermodynamical consistency imposes (Lempriere, 1968):

$$\begin{aligned} -1 &\leq \nu_{\parallel} \leq 1 \\ -\sqrt{E'_r/E'_{\parallel}} &\leq \nu_{\theta r} \leq \sqrt{E'_r/E'_{\parallel}} \cdot \\ \nu_{\parallel} &\leq 1 - 2\nu_{\theta r}^2 \frac{E'_{\parallel}}{E'_r} \end{aligned} \quad (59)$$

587 For an isotropic material of Poisson ratio ν , these inequalities reduce to $-1 \leq \nu \leq 1/2$.
 588 The case $\nu = 1/2$ corresponds to incompressible material as considered in Church (1995).

589 **A. Displacement within the shell**

590 Following the same steps as in Sec. VA, the displacement now obeys the following equa-
 591 tion:

$$\frac{d^2u}{dr^2} + \frac{2}{r} \frac{du}{dr} - \frac{2ku}{r^2} = 0, \quad (60)$$

592 with:

$$k = \frac{E'_{\parallel}(1 - \nu_{\theta r})}{E'_r(1 - \nu_{\parallel})}, \quad (61)$$

593 which is the equivalent of Eq. (9) for this purely elastic case.

594 The solutions of Eq. (60) have the form

$$u^{Tr}(r) = a^{Tr} r^{\beta_+} + b^{Tr} r^{\beta_-}, \quad (62)$$

595 with $\beta_{\pm} = \frac{1}{2}(-1 \pm \sqrt{1 + 8k})$. Note that by virtue of Eqs. (59), it can be shown that

596 $k \geq -1/8$ whatever the material properties and the exponents β_{\pm} are real. The isotropic

597 case corresponds to $k = 1$ then $\beta_- = -2$ and $\beta_+ = 1$. The variables a_T and b_T are related

598 to the boundary conditions thanks to Eq. (7):

$$a^{Tr} = \frac{(R_2 - R_{2e})R_{10}^{\beta_-} - (R_1 - R_{1e})R_{20}^{\beta_-}}{R_{10}^{\beta_-} R_{20}^{\beta_+} - R_{10}^{\beta_+} R_{20}^{\beta_-}}, \quad (63)$$

599 and

$$b^{Tr} = \frac{(R_1 - R_{1e})R_{20}^{\beta_+} - (R_2 - R_{2e})R_{10}^{\beta_+}}{R_{10}^{\beta_-} R_{20}^{\beta_+} - R_{10}^{\beta_+} R_{20}^{\beta_-}}. \quad (64)$$

600 The Rayleigh-Plesset-like equation can be derived following the same steps as in Sec. VC.

601 For the sake of simplicity we calculate directly the resonance frequency in the following

602 section.

603 B. Resonance frequency

604 Following the same steps as in Sec. VE, one gets the following system:

$$M\ddot{X} + KX = F(t), \quad (65)$$

605 where

$$X = \begin{pmatrix} x \\ y \end{pmatrix}, F(t) = \begin{pmatrix} -P_{ac}(t) \\ 0 \end{pmatrix}, M = \begin{bmatrix} 0 & \rho_f R_{20}^2 \\ 0 & 0 \end{bmatrix},$$

606 and

$$K^{Tr} = \begin{bmatrix} k_{11}^{Tr} & \frac{-2\gamma_2}{R_{20}} \\ k_{21}^{Tr} & k_{22}^{Tr} \end{bmatrix}, \text{ where}$$

$$\begin{aligned} k_{11}^{Tr} = & \left(3\kappa P_{G_0} - \frac{2\gamma_1}{R_{10}} \right) \left\{ 1 - 2 \frac{(R_{20}^{\beta_+ - 1} - R_{10}^{\beta_+ - 1})(\beta_+ - 1)^{-1} R_{10}^{\beta_-} A_+ - (R_{20}^{\beta_- - 1} - R_{10}^{\beta_- - 1})(\beta_- - 1)^{-1} R_{10}^{\beta_+} A_-}{E'_r(1 - \nu_{\parallel})(\beta_+ - \beta_-)} \right\} \\ & + \frac{2(R_{20}^{\beta_+ - 1} - R_{10}^{\beta_+ - 1})(\beta_+ - 1)^{-1} R_{10}^{\beta_-} A_+ [E'_r(1 - \nu_{\parallel})\beta_- + 2\nu_{\theta r} E'_{\parallel}]}{\left(1 - \nu_{\parallel} - 2 \frac{E'_{\parallel}}{E'_r} \nu_{\theta r}^2 \right) E'_r(1 - \nu_{\parallel})(\beta_+ - \beta_-)} \\ & - \frac{2(R_{20}^{\beta_- - 1} - R_{10}^{\beta_- - 1})(\beta_- - 1)^{-1} R_{10}^{\beta_+} A_- [E'_r(1 - \nu_{\parallel})\beta_+ + 2\nu_{\theta r} E'_{\parallel}]}{\left(1 - \nu_{\parallel} - 2 \frac{E'_{\parallel}}{E'_r} \nu_{\theta r}^2 \right) E'_r(1 - \nu_{\parallel})(\beta_+ - \beta_-)}, \end{aligned} \quad (66)$$

607 with:

$$A_+ = \beta^+(1 - \nu_{\parallel})E'_r - [1 - (2 - \beta^+)\nu_{\theta r}]E'_{\parallel}, \quad (67)$$

608

$$A_- = \beta^-(1 - \nu_{\parallel})E'_r - [1 - (2 - \beta^-)\nu_{\theta r}]E'_{\parallel}, \quad (68)$$

609 and:

$$\begin{aligned} k_{21}^{Tr} = & -3\kappa P_{G_0} + \frac{2\gamma_1}{R_{10}} \\ & + \frac{R_{20}^{\beta_+} R_{10}^{\beta_-} [E'_r(1 - \nu_{\parallel})\beta_- + 2\nu_{\theta r} E'_{\parallel}]}{\left(1 - \nu_{\parallel} - 2 \frac{E'_{\parallel}}{E'_r} \nu_{\theta r}^2 \right) (R_{10}^{\beta_-} R_{20}^{\beta_+} - R_{10}^{\beta_+} R_{20}^{\beta_-})} \\ & - \frac{R_{20}^{\beta_-} R_{10}^{\beta_+} [E'_r(1 - \nu_{\parallel})\beta_+ + 2\nu_{\theta r} E'_{\parallel}]}{\left(1 - \nu_{\parallel} - 2 \frac{E'_{\parallel}}{E'_r} \nu_{\theta r}^2 \right) (R_{10}^{\beta_-} R_{20}^{\beta_+} - R_{10}^{\beta_+} R_{20}^{\beta_-})}, \end{aligned} \quad (69)$$

610

$$k_{22}^{Tr} = \frac{R_{20} R_{10}^{\beta_- + \beta_+ - 1} [E'_r(1 - \nu_{\parallel})(\beta_+ - \beta_-)]}{\left(1 - \nu_{\parallel} - 2 \frac{E'_{\parallel}}{E'_r} \nu_{\theta r}^2 \right) (R_{10}^{\beta_-} R_{20}^{\beta_+} - R_{10}^{\beta_+} R_{20}^{\beta_-})}. \quad (70)$$

611 Then, the undamped resonance frequency is:

$$\omega_0^{Tr} = \left(\frac{\det[K^{Tr}]}{m_{12}k_{21}^{Tr}} \right)^{1/2}. \quad (71)$$

612 C. Discussion: effect of anisotropy on ω_0

613 In what follows, the couple $(E' = 2G'(1 + \nu), \nu)$ will be used to describe the elastic
 614 properties of an isotropic solid for the sake of comparison with the elastic properties of a
 615 transversely isotropic material.

616 We first discuss what is the impact of anisotropy keeping the material incompressible. In
 617 such a situation, it is shown in [Itskov and Aksel \(2002\)](#) that $\nu_{\theta r} = 1/2$ while $\nu_{\parallel} = 1 - \frac{E'_{\parallel}}{2E'_r}$.
 618 Thermodynamics constraints (Eq. (59)) then impose $E'_r > E'_{\parallel}/4$.

619 We remark that Eq. (61) becomes $k = 1$ that is, the deformation function is the same as in
 620 the isotropic case. Second, the terms in the K^{Tr} matrix implying the shell elastic constants
 621 are all proportional to E'_r and do not depend on E'_{\parallel} . We conclude that incompressible shells
 622 oscillate exactly the same way whatever the value of their in-plane Young modulus that is,
 623 they oscillate like isotropic incompressible shells of Young modulus E'_r .

624 For anisotropic compressible material, in general, hydrostatic stress does not necessarily
 625 induces a uniform dilatation in the three directions. It is interesting for comparison with
 626 the isotropic case to consider the situation where this is true. In such a situation of isotropic
 627 volumetric response, a bulk modulus can be defined as a material constant [Itskov and Aksel](#)
 628 (2002). It is equal to $\varkappa = E'_r/[3(1 - 2\nu_{\theta r})]$. In addition, it can be shown that ν_{\parallel} is given
 629 by $1 - \frac{E'_{\parallel}}{2} \left(\frac{1}{E'_r} + \frac{1}{3\varkappa} \right)$; the material properties are thus described, for the radial motion
 630 considered here, by 3 independent variables (e.g. \varkappa , E'_r and E'_{\parallel}) instead of 4 in the general

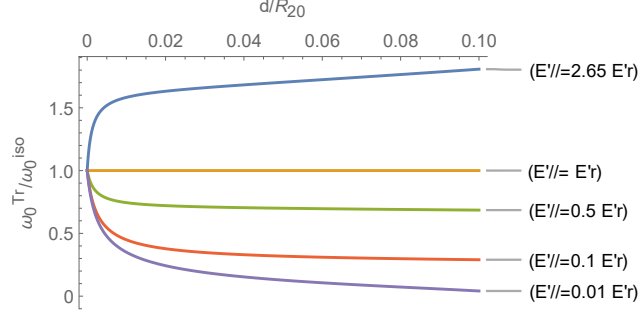


FIG. 5. Ratio of the undamped resonance frequencies in the compressible case $\omega_0^{Tr}/\omega_0^{iso}$. The values for the in-plane and out-plane Poisson ratio are $\nu_{||} = \nu_{\theta r} = 0.35$. We varied $E'_{||}$ as $0.01 E'_r$, $0.1 E'_r$, $0.5 E'_r$, E'_r and $2.65 E'_r$, the isotropic constants $E' = E'_r$ and ν are set to 88.8 MPa and 0.35 respectively.

631 case and 2 in the incompressible case. In this case also, the pulsation is that of the isotropic
 632 material of moduli $K' = \varkappa$ and $E' = E'_r$, though the deformation inside the shell is not the
 633 same: in Eq. (61), k is independent from $E'_{||}$ (but not necessarily equal to 1) and because
 634 $\nu_{||}$ appears only under the pattern $1 - \nu_{||}$ in K^{Tr} , it can be easily seen that the contribution
 635 of $E'_{||}$ vanishes.

636 Finally, in Fig. 5, we consider a general (arbitrary) case, based on the test case the
 637 configuration \mathcal{R} as it refers to a lipidic shell, which we may expect to exhibit transverse
 638 anisotropic properties. We have fixed $\nu_{||} = \nu_{\theta r} = 0.35$ and varied $E'_{||}$ as a function of E'_r ,
 639 within the bounds allowed by thermodynamics. Here, $E'_{||}$ also influences the frequency,
 640 which increases as $E'_{||}$ increases.

641 In all cases, as for the isotropic case, these results show that for a given measure of
 642 pulsation frequency, several sets of elastic parameters can yield the same result. More
 643 complex dependency with the external radius is also expected.

644 VII. CONCLUSION & PERSPECTIVES

645 We have developed a finite thickness shell model for the oscillations of an encapsulated
646 bubble whose material can be compressible and/or present different elastic properties in the
647 radial and orthoradial directions. The main hypothesis is that we have neglected the mass
648 of the shell, leading to infinite velocity for wave propagation in the material, in order to
649 simplify the equations. The next step would be to consider the complete problem of wave
650 propagation, as done for instance in ([Doinikov *et al.*, 2018](#); [Doinikov and Marmottant, 2018](#))
651 for a bubble oscillating in a liquid confined by a visco-elastic solid.

652 We have found exact expressions for the free pulsation of an encapsulated bubble, that
653 could be used to interpret more accurately experimental characterization of UCAs. Our
654 results suggest that neglecting compressibility will lead to underestimation of the shear
655 modulus, and that adding some compressibility in the model may explain the apparent
656 growth of the elastic moduli with the shell radius.

657 Due to the growing interest in the development of new generation UCAs, made of various
658 material and built with well defined radii, we expect that several opportunities to test our
659 model will emerge in the near future. Our predictions can also be used to build more
660 complete theories accounting for the response of the shells to external signals.

661 ACKNOWLEDGMENTS

662 The authors appreciated fruitful discussions with Philippe Marmottant and Salvatore
663 Federico.

664 **APPENDIX: DEFORMATION VELOCITIES**

665 We present here the expressions obtained for \dot{a} and \dot{b} by directly derivating a and b , see
 666 Sec. VB:

$$\begin{aligned} \dot{a}(t) &= \frac{R_2^2 U_2 - R_1^2 U_1}{R_3^2 - R_1^3} + \frac{U_2}{(R_2^3 - R_1^3)^2} \\ &\quad [(R_1 - R_{1e})(3R_1^2 R_2^2) - (R_2 - R_{2e})(R_2^4 + 2R_2 R_1^3)] \\ &\quad + \frac{U_1}{(R_2^3 - R_1^3)^2} \\ &\quad [(R_2 - R_{2e})(3R_1^2 R_2^2) - (R_1 - R_{1e})(R_1^4 + 2R_1 R_2^3)], \end{aligned}$$

667 and:

$$\begin{aligned} \dot{b}(t) &= \frac{(R_2 U_1 - R_1 U_2) R_1^2 R_2^2}{R_3^2 - R_1^3} + \frac{U_1}{(R_2^3 - R_1^3)^2} \\ &\quad [(R_1 - R_{1e})(2R_1 R_2^6 + R_1^4 R_2^3) - (R_2 - R_{2e})(3R_1^2 R_2^5)] \\ &\quad + \frac{U_2}{(R_2^3 - R_1^3)^2} \\ &\quad [(R_2 - R_{2e})(2R_2 R_1^6 + R_2^4 R_1^3) - (R_1 - R_{1e})(3R_1^5 R_2^2)]. \end{aligned}$$

668 ¹Note that $\nu_{r\theta}$ is used by some authors instead of $\nu_{\theta r}$ (Lempriere, 1968).

669

670 Abou-Saleh, R. H., Peyman, S. A., Critchley, K., Evans, S. D., and Thomson, N. H. (2013).

671 “Nanomechanics of lipid encapsulated microbubbles with functional coatings,” *Langmuir*

672 **29**(12), 4096–4103.

673 Altenbach, H., Brigadnov, I. A., and Eremeyev, V. A. (2008). “Oscillations of a

674 magneto-sensitive elastic sphere,” *ZAMM-Journal of Applied Mathematics and Mechan-*

675 ics/*Zeitschrift für Angewandte Mathematik und Mechanik: Applied Mathematics and Me-*
676 *chanics* **88**(6), 497–506.

677 Besant, W. H. (1859). *A Treatise on Hydrostatics and Hydrodynamics* (Deighton, Bell).

678 Buchner Santos, E., Morris, J. K., Glynos, E., Sboros, V., and Koutsos, V. (2012).
679 “Nanomechanical properties of phospholipid microbubbles,” *Langmuir* **28**(13), 5753–5760.

680 Campbell, S., Griffin, D. R., Pearce, J. M., Diaz-Recasens, J., Cohen-Overbeek, T., Willson,
681 K., and Teague, M. J. (1983). “New doppler technique for assessing uteroplacental blood
682 flow,” *The Lancet* **321**(8326), 675–677.

683 Chatterjee, D., and Sarkar, K. (2003). “A newtonian rheological model for the interface of
684 microbubble contrast agents,” *Ultrasound Med. Biol.* **29**(12), 1749–1757.

685 Chetty, K., Stride, E., Sennoga, C. A., Hajnal, J. V., and Eckersley, R. J. (2008). “High-
686 speed optical observations and simulation results of sonovue microbubbles at low-pressure
687 insonation,” *IEEE trans. ultrason. ferr. frequ. control* **55**(6), 1333–1342.

688 Church, C. C. (1995). “The effects of an elastic solid surface layer on the radial pulsations
689 of gas bubbles,” *J. Ac. Soc. Am.* **97**(3), 1510–1521.

690 Coupier, G., Djellouli, A., and Quilliet, C. (2019). “Let’s deflate that beach ball,” *Eur.*
691 *Phys. J. E* **42**(9), 129.

692 Dalenbring, M. (2002). “An explicit formulation of a three-dimensional material damping
693 model with transverse isotropy,” *Int. J. Sol. Struct.* **39**(1), 225 – 249.

694 De Jong, N., Cornet, R., and Lancee, C. (1994). “Higher harmonics of vibrating gas-filled
695 microspheres. part one: simulations,” *Ultrasonics* **32**(6), 447–453.

696 de Jong, N., and Hoff, L. (1993). “Ultrasound scattering properties of albumex micro-
697 spheres,” *Ultrasonics* **31**(3), 175–181.

698 de Jong, N., Hoff, L., Skotland, T., and Bom, N. (1992). “Absorption and scatter of en-
699 capsulated gas filled microspheres: theoretical considerations and some measurements,”
700 *Ultrasonics* **30**(2), 95–103.

701 Doinikov, A. A., and Dayton, P. A. (2006). “Spatio-temporal dynamics of an encapsulated
702 gas bubble in an ultrasound field,” *J. Ac. Soc. Am.* **120**(2), 661–669.

703 Doinikov, A. A., Dollet, B., and Marmottant, P. (2018). “Model for the growth and the
704 oscillation of a cavitation bubble in a spherical liquid-filled cavity enclosed in an elastic
705 medium,” *Phys. Rev. E* **97**, 013108.

706 Doinikov, A. A., Haac, J. F., and Dayton, P. A. (2009). “Modeling of nonlinear viscous
707 stress in encapsulating shells of lipid-coated contrast agent microbubbles,” *Ultrasonics*
708 **49**(2), 269–275.

709 Doinikov, A. A., and Marmottant, P. (2018). “Natural oscillations of a gas bubble in a
710 liquid-filled cavity located in a viscoelastic medium,” *J. Sound Vib.* **420**, 61–72.

711 Dovstam, K. (1995). “Augmented hooke’s law in frequency domain. a three dimensional,
712 material damping formulation,” *International Journal of Solids and Structures* **32**(19),
713 2835–2852.

714 Errico, C., Pierre, J., Pezet, S., Desailly, Y., Lenkei, Z., Couture, O., and Tanter, M. (2015).
715 “Ultrafast ultrasound localization microscopy for deep super-resolution vascular imaging,”
716 *Nature* **527**, 499-502.

717 Faez, T., Goertz, D., and De Jong, N. (2011). “Characterization of Definity ultrasound
718 contrast agent at frequency range of 5-15 Mhz,” *Ultrasound Med. Biol.* **37**(2), 338–342.

719 Goertz, D. E., de Jong, N., and van der Steen, A. F. (2007). “Attenuation and size distribu-
720 tion measurements of Definity and manipulated Definity populations,” *Ultrasound Med.*
721 *Biol.* **33**(9), 1376-1388.

722 Gong, Y., Cabodi, M., and Porter, T. M. (2014). “Acoustic investigation of pressure-
723 dependent resonance and shell elasticity of lipid-coated monodisperse microbubbles,” *Ap-*
724 *plied Physics Letters* **104**(7), 074103.

725 Gorce, J.-M., Arditi, M., and Schneider, M. (2000). “Influence of bubble size distribution
726 on the echogenicity of ultrasound contrast agents: A study of sonovue,” *Invest. Radiol.*
727 **35**(11), 661–671.

728 Gramiak, R., and Shah, P. M. (1968). “Echocardiography of the aortic root,” *Invest. Radiol.*
729 **3**(5), 356–366.

730 Guillot, F. M., and Trivett, D. H. (2011). “Complete elastic characterization of viscoelastic
731 materials by dynamic measurements of the complex bulk and young’s moduli as a function
732 of temperature and hydrostatic pressure,” *J. Sound Vib.* **330**(14), 3334–3351.

733 Helfield, B. (2019). “A review of phospholipid encapsulated ultrasound contrast agent mi-
734 crobubble physics,” *Ultrasound Med. Biol.* **45**(2), 282–300.

735 Helfield, B., Leung, B. Y., Huo, X., and Goertz, D. (2014). “Scaling of the viscoelastic
736 shell properties of phospholipid encapsulated microbubbles with ultrasound frequency,”
737 *Ultrasonics* **54**(6), 1419–1424.

738 Helfield, B. L., and Goertz, D. E. (2013). “Nonlinear resonance behavior and linear shell
739 estimates for Definity and Micromarker assessed with acoustic microbubble spectroscopy,”
740 J. Ac. Soc. Am. **133**(2), 1158–1168.

741 Hoff, L., Sontum, P. C., and Hovem, J. M. (2000). “Oscillations of polymeric microbubbles:
742 Effect of the encapsulating shell,” J. Ac. Soc. Am. **107**(4), 2272–2280.

743 Hu, H., Zhou, H., Du, J., Wang, Z., An, L., Yang, H., Li, F., Wu, H., and Yang, S. (2011).
744 “Biocompatible hollow silica microspheres as novel ultrasound contrast agents for in vivo
745 imaging,” J. Mater. Chem. **21**, 6576–6583.

746 Hutchinson, J. W. (1967). “Imperfection sensitivity of externally pressurized spherical
747 shells,” ASME. J. Appl. Mech. **34**, 49–55.

748 Itskov, M., and Aksel, N. (2002). “Elastic constants and their admissible values for incom-
749 pressible and slightly compressible anisotropic materials,” Acta Mech. **157**, 81-96.

750 Khismatullin, D. B., and Nadim, A. (2002). “Radial oscillations of encapsulated microbub-
751 bles in viscoelastic liquids,” Physics of Fluids **14**(10), 3534–3557.

752 Lakes, R. S., and Wineman, A. (2006). “On poisson’s ratio in linearly viscoelastic solids,”
753 J. Elast. **85**(1), 45–63.

754 Landau, L., and Lifschitz, E. (1986). *Theory of Elasticity*, 3rd ed. (Elsevier Butterworth-
755 Heinemann, Oxford).

756 Landau, L., and Lifschitz, E. (1987). *Fluid Mechanics.*, 2nd ed. (Elsevier Butterworth-
757 Heinemann, Oxford).

758 Langtangen, H. P., and Pedersen, G. K. (2016). *Scaling of differential equations* (Springer
759 International Publishing Berlin, Germany:).

760 Lemaitre, J., and Chaboche, J.-L. (1994). *Mechanics of solid materials* (Cambridge univer-
761 sity press).

762 Lempriere, B. M. (1968). “Poisson’s ratio in orthotropic materials,” *AIAA Journal* **6**(11),
763 2226–2227.

764 Li, Q., Matula, T. J., Tu, J., Guo, X., and Zhang, D. (2013). “Modeling complicated
765 rheological behaviors in encapsulating shells of lipid-coated microbubbles accounting for
766 nonlinear changes of both shell viscosity and elasticity,” *Physics Med. Biol.* **58**(4), 985.

767 Linn, J., Lang, H., and Tuganov, A. (2013). “Derivation of a viscoelastic constitutive model
768 of kelvin-voigt type for cosserat rods,” *Mech. Sci.* **4**, 79–96.

769 Liu, B., Zhou, X., Yang, F., Shen, H., Wang, S., Zhang, B., Zhi, G., and Wu, D. (2014).
770 “Fabrication of uniform sized polylactone microcapsules by premix membrane emulsifica-
771 tion for ultrasound imaging,” *Polym. Chem.* **5**, 1693–1701.

772 Lubarda, V., and Chen, M. C. (2008). “On the elastic moduli and compliances of trans-
773 versely isotropic and orthotropic materials,” *J. Mech. Mat. Struct.* **3**, 153–171.

774 Lubarda, V. A., and Asaro, R. J. (2014). “Viscoelastic response of anisotropic biological
775 membranes. part II: Constitutive models,” *Theor. Appl. Mech.* **41**, 213–231.

776 Lum, J. S., Dove, J. D., Murray, T. W., and Borden, M. A. (2016). “Single microbubble
777 measurements of lipid monolayer viscoelastic properties for small-amplitude oscillations,”
778 *Langmuir* **32**(37), 9410–9417.

779 Lytra, A., Sboros, V., Giannakopoulos, A., and Pelekasis, N. (2020). “Modeling atomic
780 force microscopy and shell mechanical properties estimation of coated microbubbles,” *Soft*
781 *Matter* **16**(19), 4661–4681.

782 Marmottant, P., van der Meer, S., Emmer, M., Versluis, M., de Jong, N., Hilgenfeldt, S., and
783 Lohse, D. (2005). “A model for large amplitude oscillations of coated bubbles accounting
784 for buckling and rupture,” *J. Ac. Soc. Am.* **118**, 3499–3505.

785 Mohanty, K., Papadopoulou, V., Newsome, I. G., Shelton, S., Dayton, P. A., and Muller,
786 M. (2019). “Ultrasound multiple scattering with microbubbles can differentiate between
787 tumor and healthy tissue in vivo,” *Phys. Med. Biol.* **64**, 115022.

788 Morgan, K. E., Allen, J. S., Dayton, P. A., Chomas, J. E., Klibaov, A., and Ferrara,
789 K. W. (2000). “Experimental and theoretical evaluation of microbubble behavior: Effect
790 of transmitted phase and bubble size,” *IEEE trans. ultrason. ferr. frequ. control* **47**(6),
791 1494–1509.

792 Munglani, G., Wittel, F. K., Vetter, R., Bianchi, F., and Herrmann, H. J. (2019). “Collapse
793 of orthotropic spherical shells,” *Phys. Rev. Lett.* **123**, 058002.

794 Parrales, M. A., Fernandez, J. M., Perez-Saborid, M., Kopechek, J. A., and Porter, T. M.
795 (2014). “Acoustic characterization of monodisperse lipid-coated microbubbles: Relation-
796 ship between size and shell viscoelastic properties,” *The Journal of the Acoustical Society*
797 *of America* **136**(3), 1077–1084.

798 Paul, S., Katiyar, A., Sarkar, K., Chatterjee, D., Shi, W. T., and Forsberg, F. (2010).
799 “Material characterization of the encapsulation of an ultrasound contrast microbubble
800 and its subharmonic response: Strain-softening interfacial elasticity model,” *The Journal*
801 *of the Acoustical Society of America* **127**(6), 3846–3857.

802 Paul, S., Russakow, D., Rodgers, T., Sarkar, K., Cochran, M., and Wheatley, M. A.
803 (2013). “Determination of the interfacial rheological properties of a poly (DL-lactic acid)-

804 encapsulated contrast agent using in vitro attenuation and scattering,” *Ultrasound Med.*
805 *Biol.* **39**(7), 1277–1291.

806 Pitois, O., Buisson, M., and Chateau, X. (2015). “On the collapse pressure of armored
807 bubbles and drops,” *Eur. Phys. J. E* **38**(5), 48.

808 Plesset, M. S., and Prosperetti, A. (1977). “Bubble dynamics and cavitation,” *Ann. Rev.*
809 *Fluid Mech.* **9**(1), 145–185.

810 Pritz, T. (2009). “Relation of bulk to shear loss factor of solid viscoelastic materials,”
811 *Journal of sound and vibration* **324**(3-5), 514–519.

812 Prosperetti, A. (1987). “The equation of bubble dynamics in a compressible liquid,” *The*
813 *Physics of fluids* **30**(11), 3626–3628.

814 Quemeneur, F., Quilliet, C., Faivre, M., Viallat, A., and Pépin-Donat, B. (2012). “Gel
815 phase vesicles buckle into specific shapes,” *Phys. Rev. Lett.* **108**, 108303.

816 Quilliet, C. (2012). “Numerical deflation of beach balls with various poisson’s ratios: from
817 sphere to bowl’s shape,” *Eur. Phys. J. E* **35**, 48.

818 Rayleigh, L. (1917). “Viii. on the pressure developed in a liquid during the collapse of a
819 spherical cavity,” *The London, Edinburgh, and Dublin Philosophical Magazine and Journal*
820 *of Science* **34**(200), 94–98.

821 Sarkar, K., Shi, W. T., Chatterjee, D., and Forsberg, F. (2005). “Characterization of ul-
822 trasound contrast microbubbles using in vitro experiments and viscous and viscoelastic
823 interface models for encapsulation,” *J. Ac. Soc. Am.* **118**(1), 539–550.

824 Segers, T., de Rond, L., de Jong, N., Borden, M., and Versluis, M. (2016). “Stability of
825 monodisperse phospholipid-coated microbubbles formed by flow-focusing at high produc-

tion rates,” *Langmuir* **32**(16), 3937–3944.

Segers, T., Gaud, E., Casqueiro, G., Lassus, A., Versluis, M., and Frinking, P. (2020). “Foam-free monodisperse lipid-coated ultrasound contrast agent synthesis by flow-focusing through multi-gas-component microbubble stabilization,” *Applied Physics Letters* **116**(17), 173701.

Shafi, A. S., McClements, J., Albaijan, I., Abou-Saleh, R. H., Moran, C., and Koutsos, V. (2019). “Probing phospholipid microbubbles by atomic force microscopy to quantify bubble mechanics and nanostructural shell properties,” *Colloids Surf. B* **181**, 506–515.

Song, R., Peng, C., Xu, X., Wang, J., Yu, M., Hou, Y., Zou, R., and Yao, S. (2018). “Controllable formation of monodisperse polymer microbubbles as ultrasound contrast agents,” *ACS Appl. Mat. Int.* **10**(17), 14312–14320.

Thompson, W., and Kelvin, L. (1865). “On the elasticity and viscosity of metals,” *Proc. Roy. Soc. London A* **14**(289-297), 1.

Tschoegl, N., Knauss, W. G., and Emri, I. (2002). “Poisson’s ration in linear viscoelasticity - a critical review ,” *Mech. Time-Dep. Mat.* **6**, 3.

Tsiglifis, K., and Pelekasis, N. A. (2008). “Nonlinear radial oscillations of encapsulated microbubbles subject to ultrasound: The effect of membrane constitutive law,” *J. Ac. Soc. Am.* **123**(6), 4059–4070.

Tu, J., Guan, J., Qiu, Y., and Matula, T. J. (2009). “Estimating the shell parameters of sonovue® microbubbles using light scattering,” *J. Ac. Soc. Am.* **126**(6), 2954–2962.

Tu, J., Swalwell, J. E., Giraud, D., Cui, W., Chen, W., and Matula, T. J. (2011). “Microbubble sizing and shell characterization using flow cytometry,” *IEEE trans. ultrason.*

848 ferr. frequ. control **58**(5), 955–963.

849 van der Meer, S. M., Dollet, B., Voormolen, M. M., Chin, C. T., Bouakaz, A., de Jong,
850 N., Versluis, M., and Lohse, D. (2007). “Microbubble spectroscopy of ultrasound contrast
851 agents,” *J. Ac. Soc. Am.* **121**(1), 648–656.

852 van Rooij, T., Luan, Y., Renaud, G., van der Steen, A. F., Versluis, M., de Jong, N.,
853 and Kooiman, K. (2015). “Non-linear response and viscoelastic properties of lipid-coated
854 microbubbles: DSPC versus DPPC,” *Ultrasound in medicine & biology* **41**(5), 1432–1445.

855 Versluis, M., Stride, E., Lajoinie, G., Dollet, B., and Segers, T. (2020). “Ultrasound Con-
856 trast Agent Modeling: A Review,” *Ultrasound in medicine & biology* **46**(9), 2117 - 2144.

857 Vilov, S., Arnal, B., and Bossy, E. (2017). “Overcoming the acoustic diffraction limit in
858 photoacoustic imaging by the localization of flowing absorbers,” *Opt. Lett.* **42**, 4379–4382.

859 Vincent, O., and Marmottant, P. (2017). “On the statics and dynamics of fully confined
860 bubbles,” *J. Fluid Mech.* **827**, 194–224.

861 Voigt, W. (1892). “Ueber innere reibung fester körper, insbesondere der metalle,” *Annalen
862 der Physik* **283**(12), 671–693.

863 von Ende, S., Lion, A., and Lammering, R. (2011). “On the thermodynamically consistent
864 fractional wave equation for viscoelastic solids,” *Acta Mech.* **221**, 1-10.

865 Wang, Q., Xue, C., Qin, Y., Zhang, X., Li, Y. *et al.* (2020). “The fabrication of protein
866 microbubbles with diverse gas core and the novel exploration on the role of interface
867 introduction in protein crystallization,” *Colloids and Surfaces A: Physicochemical and
868 Engineering Aspects* 124471.

869 Wang, Q. X. (2017). "Oscillation of a bubble in a liquid confined in an elastic solid," Phys.
870 Fluids **29**, 072101.